**Bromine soil/sediment enrichment in tidal salt marshes as a potential indicator of climate changes driven by solar activity: new insights from W coast Portuguese estuaries**

J. Moreno[a,b,1], F. Fatela[a,b], E. Leorri[c], F. Moreno[d], M.C. Freitas[a,b], T. Valente[e], M.F. Araújo[f], J.J. Gómez-Navarro[g], L. Guise[e] and W.H. Blake[h]

[a] IDL - Instituto Dom Luiz, Universidade de Lisboa, Campo Grande, 1749-016 Lisboa, Portugal.

[b] Departamento de Geologia da Faculdade de Ciências da Universidade de Lisboa, Campo Grande, 1749-016 Lisboa, Portugal.

[c] East Carolina University, Department of Geological Sciences, Greenville, NC 27858-4353, USA.

[d] Independent researcher, Caminho da Portela, 97, 4940-061 Bico PCR, Portugal.

[e] Universidade do Minho, Centro de Investigação Geológica, Ordenamento e Valorização de Recursos, Departamento de Ciências da Terra, CIG-R, 4710-057 Braga, Portugal.

[f] Universidade de Lisboa, Instituto Superior Técnico, Centro de Ciências e Tecnologias Nucleares (C$^2$TN), Estrada Nacional 10, km 139,7, 2695-066 Bobadela LRS, Portugal.

[g] Department of Physics, University of Murcia, Spain.

[h] School of Geography, Earth and Environmental Sciences, Plymouth University, Plymouth, Devon, PL4 8AA, UK

---

[1] jcmoreno@fc.ul.pt

22

## Abstract

This paper aims at providing insight about bromine (Br) cycle in four Portuguese estuaries: Minho, Lima (in the NW coast) and Sado, Mira (in the SW coast). The focus is on their tidal marsh environments, quite distinct with regard to key biophysicochemical attributes. Regardless of the primary bromide ($Br^-$) common natural source, i.e. seawater, the NW marshes present relatively higher surface soil/sediment Br concentrations than the ones from SW coast. This happens in close relation with organic matter (OM) content, and is controlled by their main climatic context. Yet, the anthropogenic impact on Br concentrations cannot be discarded. Regarding [Br] spatial patterns across the marshes, the results show a general increase from tidal flat towards high marsh. Maxima [Br] occur in the upper driftline zone, at transition from highest low marsh to high marsh, recognized as a privileged setting for OM accumulation. Based on the discovery of OM ubiquitous bromination in marine and transitional environments, it is assumed that this Br occurs mainly as organobromine. Analysis of two dated sediment cores indicates that, despite having the same age (AD 1300), the Caminha salt marsh (Minho estuary) evidences higher Br enrichment than the Casa Branca salt marsh (Mira estuary). This is related to a greater Br storage ability, which is linked to OM build-up and rate dynamics under different climate scenarios. Both cores evidence a fairly similar temporal Br enrichment pattern, and may be interpreted in light of the sun–climate coupling. Thereby, most of the well-known Grand Solar Minima during the Little Ice Age appear to have left an imprint on these marshes, supported by higher [Br] in soils/sediments. Besides climate changes driven by solar activity and impacting marsh Br biogeodynamics, those [Br] positive peaks might also reflect inputs of enhanced volcanic activity covarying with Grand Solar Minima.

46

## 1. Introduction

Wetlands play an important role on the biogeochemical cycle of elements such as carbon, nitrogen, phosphorus, sulphur and mercury at local, regional and even global scales (e.g., Marques et al., 2011; Neubauer et al., 2013). A considerable amount of research has revealed that this is also true for bromine (Br) (Varner et al., 1999; Keppler et al., 2000; Rhew et al., 2000, 2002, 2014; Dimmer et al., 2000; Drewer et al., 2006; Manley et al., 2006; Hardacre et al., 2009, 2013; Blei et al., 2010; Martínez-Cortizas et al., 2007, 2016). Specifically, coastal wetlands, in which tidal marshes are included, represent important land-ocean-atmosphere interfaces that allow to capture spatiotemporal variability in chemical fluxes. In these habitats, Br mainly supplied by seawater interacts with both halophytes and the relatively large pool of soil/sediment organic matter (OM). This connection occurs through, although still poorly understood, bromination processes that contribute to the production of organobromine compounds, which have detrimental effects on the atmosphere. For instance, salt marshes have been identified as globally significant natural sources of methyl bromide ($CH_3Br$) (Rhew et al., 2014, and references therein), a reactive trace gas contributing to ozone loss processes in the stratosphere (e.g., Chipperfield, 2015). On the other hand, significant widespread bromination of natural OM may significantly impact the preservation and/or degradation of organic carbon ($C_{org}$) in soils/sediments (Leri and Myneni, 2012), therefore affecting the recognized salt marsh ecosystem's role on climate and carbon sequestration. It is also known that in coastal (and open ocean) areas, bromine-radical chemistry provides alternative reaction pathways in the marine atmospheric boundary layer for (i) sulphur cycling, with associated implications for

3

72 aerosol production (and growth), radiative heat transfer and climate (Keene et al., 2007),

73 and (ii) mercury (Hg) cycling (Obrist et al., 2011; Tas et al., 2012), with Br-induced mercury

74 oxidation as a likely important Hg source to world's oceans, which can contribute to human

75 mercury exposure by seafood consumption (Sunderland, 2007). Taking together the

76 previous findings about the Br influence on other key element biogeochemical cycles in the

77 marine domain, and the knowledge that natural $CH_3Br$ emissions are contributing to

78 increase the stratospheric reactive Br budget (e.g., Carpenter et al., 2014), establishing the

79 foundations of the Br biogeochemical cycle in coastal areas and tidal marsh habitats has

80 gained a renewed significance.

81 Traditionally, Br has been used in conjunction with chlorine (Cl) as a geochemical proxy for

82 seawater intrusion in coastal areas (e.g., Jones et al., 1999; Alcalá and Custodio, 2008),

83 and alone as a paleosalinity indicator and a stratigraphic marker in brine cores (Adams,

84 1969; Ziegler et al., 2008). An alternative interpretation regarding Br concentrations and

85 fluxes has been proposed by Moreno et al. (2015) when studying the sedimentary record

86 recovered from the high marsh zone on a tidal salt marsh located in the NW coast of

87 Portugal (Caminha, in the Minho River estuary). They suggested that the most prominent Br

88 enrichment peaks between AD 1300 (tidal marsh settlement) and AD 1800 (considered as

89 the beginning of industrialization) were primarily driven by a series of biogeochemical

90 processes rather than an indication of seawater intrusion events in the Minho estuary.

91 Those processes responded to significantly prolonged environmental (e.g., temperature and

92 precipitation) shifts triggered by Grand Minima Episodes of solar activity (SA) during the

93 LIA, namely the Wolf and the Maunder Minima, as well as the Dalton Minimum. These

94 episodes corresponded to periods of solar minimal energy output, as demonstrated by long-

95 term records of SA proxies (e.g. Usoskin et al., 2007), affecting Earth's climate. Prolonged

96 changes in environmental conditions can lead to significant responses at all levels of

97 ecosystem organization, generating persistent alterations in its biogeochemical functioning

4

(e.g., Keller et al., 2006; Neubauer et al., 2013). Accordingly, and based on Moreno et al. (2015) that linked Br biogeodynamics to past SA, the impact of the sun–climate coupling at Grand Solar Minima resulted in cascading effects on Br cycling in the Caminha salt marsh, in parallel with rate changes in OM bromination, which ultimately weakened the marsh's role as a source for $CH_3Br$.

Following the study conducted in Caminha, the current contribution expands and generalises the analysis, including three other Portuguese estuaries (Figure 1): the Lima estuary, also in the NW coast, and the Sado and Mira estuaries, both located in the SW coast. Broadly, the Portuguese W coast is typically characterized by an Atlantic climate, though two main climatic regions can be distinguished. Compared to the NW coast, climate in SW coast has drier summers, lower annual precipitation as well as higher annual temperatures and insolation. Therefore, the aim of this work is twofold: (i) acquire a wider latitudinal range of Br measurements in waters (superficial and interstitial) and marsh soils/sediments in order to infer trends associated to the bio-geomorphological settings and climatic variability, and (ii) improve the understanding of bromine-climate relationships driven by SA, also providing new independent data and source insight to the still ongoing debate about the "missing source" for the $CH_3Br$ global budget (Yvon-Lewis et al., 2009).


## 2. Regional setting

*NW coast*

Taken together, the Minho and Lima watersheds cover an area of 19 550 $km^2$ under an Atlantic wet climate, with relatively high exposition to maritime winds, high mean annual precipitations (Minho: 1200–2400 mm; Lima:  1300–4200 mm), mild summers (summer

121     mean temperatures from ca. 18–22ºC) and relatively low mean annual insolation (2200–

122     2500 hours) (APA, 2011).

123     The Minho estuary (23 km$^2$) is oriented NE–SW and presents a semidiurnal, high-mesotidal

124     regime in which vertical stratification occurs during periods of large freshwater discharge.

125     The mean annual freshwater inflow is around 300 m$^3$/s (Ferreira et al., 2003). The highest

126     high water spring (HHWS) is 4 m height, but this is often amplified by storm surges

127     (Taborda and Dias, 1991), which we observed during field work. The mean tidal range is of

128     about 2.0 m. The upstream limit of the tidal salt wedge in the Minho River is 9 km (Fatela et

129     al., 2009). Large tidal flat and tidal marsh surfaces with approximately 6 km$^2$ occur in the

130     Minho estuary's banks, with its largest expansion along the left bank – Caminha tidal marsh

131     (ca. 2.5 km$^2$) – at the confluence with Coura tributary (Figure 1). Recently, Reis et al. (2014)

132     updated the estuary ecological quality to "moderately to remarkably polluted" based on

133     metal concentrations guidelines (SFT TA-1467/1997). Furthermore, the use of ethylene

134     dibromide in leaded gasoline and the vehicle emissions since 1930, a shared Br and Pb

135     anthropogenic source, appears to have had a significant impact on the Caminha salt marsh

136     (Moreno et al., 2015).

137     The Lima estuary (5 km$^2$), located 20 km south of Minho, is oriented ENE–WSW and it is a

138     semidiurnal mesotidal estuary, with a mean tidal range of about 2.5 m and a HHWS of 3.7

139     m (Vale and Dias, 2011). The mean annual freshwater inflow is 50 m$^3$/s (Vale and Dias,

140     2011). Here the tidal salt wedge effect is noticed to 3–5 km upstream in winter and no more

141     than 15 km in summer (Alves, 2003). Intertidal areas extend over more than 2 km$^2$ on the

142     banks of the Lima estuary, including the Nossa Senhora do Rosário salt marsh (NSR;

143     Figure 1). The Lima lower estuary's ecological status is considered moderate (Costa-Dias et

144     al., 2010). This results from the significant impact on the estuary of the harbour activities,

145     leading to continuous petrochemical contamination (Lima et al., 2007), and diffuse pollution

from agriculture, domestic, and industrial waste discharges, including a paper mill (Costa-Dias et al., 2010).

The salt marshes of these two NW sites are classified as Eurosiberian, based on their plant communities (Costa et al., 2009), with abundant reed meadows where the presence of *Juncus maritimus* Lam. (C3 plant; non-succulent; perennial) is ubiquitous (Honrado et al., 2004; Almeida et al., 2011). Although, other plant species can also be found such as the non-native *Triglochin striatum* Ruiz & Pav. (C3 plant; succulent; perennial), the invasive *Phragmites australis* (Cav.) Trin ex. Steud. (C3 plant) and the weed *Spartina patens* (Aiton) Muhl (C4 plant; non-succulent; perennial) (Almeida et al., 2011).

### *SW coast*

The SW coast of Portugal, where the Sado and Mira estuaries are located, is under a sub-wet Mediterranean climate, with mean values of annual precipitation around 600–700 mm (Bettencourt et al., 2003). Mean air surface temperatures are near 23⁰C in the hottest months (July and August), with a yearly average number of sunshine hours ranging 2900–3000 (APA, 2011), also showing almost permanent maritime moist winds (APA, 2011). The size of Sado and Mira rivers watersheds is 6 700 $km^2$ and 1 576 $km^2$, respectively.

The Sado estuary (170 $km^2$), the second largest estuarine system in Portugal, is located about 40 km south of Lisbon (Figure 1). It is a well-mixed estuary under normal river flow conditions, however, high discharge in some winter months may cause moderate stratification locally (Ferreira et al., 2003). It has a complex morphology generally oriented NW–SE and presents wide tidal flats as well as narrow and discontinuous coastal salt marshes covering around 7.2 $km^2$ (Moreira, 1992). The tidal pattern is semi-diurnal, with a mean tidal range of about 2.7 m and a HHWS of 3.2 m (Martins et al., 2001). The maximum

170    salt-wedge limit is 70 km upstream. The mean annual freshwater input is ca. 40 m$^3$/s,

171    exhibiting large interannual fluctuations. The lower estuary behaves as a coastal lagoon,

172    while the upper reaches present a greater fluvial influence (Martins et al., 2001). In general,

173    the Sado estuary can be classified as moderately contaminated, but the lower estuary and

174    some segments near industrial areas have revealed levels of concern for several

175    contaminants both organic and inorganic, with adverse toxicological effects to biota (e.g.,

176    Neuparth et al., 2005).

177    Finally, the vertically well-mixed Mira estuary (4.5 km$^2$) is a narrow incised estuary oriented

178    NE–SW (e.g., Paula et al., 2006). It presents a semi-diurnal mesotidal regime with a mean

179    tidal range of about 2.4 m and a HHWS of 3.5 m (Amaral et al., 2007). The salt edge may

180    reach 32 km from the river mouth (Bettencourt et al., 2003). The lower section of the estuary

181    has a dominant marine influence due to low, seasonal and limited freshwater input by the

182    Mira River (2.9 m$^3$/s). This characteristic has allowed the development in the lower 8 km of

183    large, intertidal, and homogenous seagrass meadows of *Zostera noltii* Hornemann, 1832

184    (e.g., Cunha et al., 2013). The estuarine area is also characterized by bare sandy areas and

185    muddy substrates, with a 2.9 km$^2$ area of fringing salt marshes occurring as far as 15–20

186    km upstream (Costa et al., 2001). These salt marshes have remained nearly unchanged

187    since 1958, with the entire ecosystem relatively undisturbed by anthropogenic activities

188    (Castro and Freitas, 2006).

189    As oppose to the NW sites, the SW salt marshes studied here belong to the Biogeographic

190    Mediterranean region (Costa et al., 2009). The halophytic community is mixed including

191    perennial succulent species such as *Halimione portulacoides* (L.) Aellen (C3 plant),

192    *Sarcocornia fruticosa* (L.) A.J. Scott (C3 plant), *Sarcocornia perennis* (Mill.) A.J. Scott (C3

193    plant) in the high marsh and the annuals *Spartina maritima* (Curtis) Fernald (C4 plant) and

194    *Salicornia fragilis* P. W. Ball & Tutin (C3 plant) in the low marsh (e.g., Costa, 2001).

195

## 2. Materials and Methods

### 2.1. Water and sediment samples

The methodologies used for sampling and analysis of water (superficial and interstitial) and sediments (surface and cored) in the Lima, Sado and Mira estuaries follow Moreno et al. (2015) and are fully described therein. Figure 1 and Tables 1 and 2 summarize the new samples analysed here: eight interstitial water samples from three salt marsh transects (NSR_L, TRO_S, PMF_M), ninety-one sediment surface samples from the intertidal domain (tidal flat, devoid of vascular plants; low marsh and high marsh zones with typical halophytic vegetation), along ten cross-shore transects, as well as an one-metre-long sediment core (hereafter FWCBr) recovered with a manual Auger sampler from the Casa Branca salt marsh (1.74 m above mean sea level; 37°40′03.7″ N and 8°43′12.7″ W), located on the Mira River estuary. A total of thirty sliced (1 cm thick) samples were analysed for Br and OM contents. The FCPw1 core from Moreno et al. (2015), located in the Caminha high marsh zone (1.55 m above mean sea level; 41°52′37.0″ N and 8°49′28.0″ W), is also indicated in Figure 1.

In order to characterize the two possible end-members (fluvial and marine) of biogeochemical sources to salt marshes, four marine seawater and four fluvial freshwater samples were collected (Table 1).

Water sample analyses: The filtrate was analysed for bromide (Br⁻), amongst other anions, by ion chromatography (IC) with suppressed conductivity detection (761 Compact IC Metrohm), and raw data processed with Metrohm Metro data 1.1. The IC method no. S-73, developed by Metrohm to determine anions in seawater, was used for the most saline waters (see Valente et al., 2009 and Moreno et al., 2015 for detailed information). A set of

standards was prepared to make a 6-point calibration curve covering the range of Br⁻ (and Cl⁻) concentrations in water samples. The IC method not only allows an efficient separation of the Br⁻ and Cl⁻ peaks, but has also the advantage of measuring both anions in the same sample preventing the errors introduced by dilution. A standard (20 mg/L) was run independently of the calibration curve to check for accuracy (every two samples) and sample replicates were run to check for precision. The precision was within the relative standard deviation (RSD) of 5% for all determinations and results were accurate within precision.

Sediment sample analysis: Br concentrations in cored samples, along with the collected surface sediments, were determined by Energy-Dispersive X-Ray Fluorescence Spectrometry (EDXRF), using a KEVEX 771 spectrometer. To calibrate the spectrometer and verify the accuracy and precision of the overall procedure three certified reference materials were analysed: SGR1 (Green River Shale from the United States Geological Survey – USGS), SRM 2704 (Buffalo River Sediment) and SRM1646 (Estuarine Sediment), both from the National Institute for Standards and Technology (NIST). A complete description of the equipment, analytical conditions and spectral evaluation, along with the calibration and quantification techniques, is available in Araújo et al. (1998, 2003). Accuracy and precision on the Br determinations are better than 10% as previously fully described in Moreno et al. (2015). The OM content was determined as Loss-on-Ignition (LOI), with an aliquot of bulk sediment sample (2.0 g) dried and oven-heated at a temperature of 500 ºC ± 50 ºC for about 2 hours (Moreira et al., 2009). Quality control was checked by replicate analysis (40% of the total), with errors lying in the interval 0.1%–15.0% (average: 5.7%) of the measured value. In an attempt to test the reliability of LOI data for the estimation of $C_{org}$ content, a regression analysis was performed for LOI *vs.* $C_{org}$ for the FCPw1 core, with $C_{org}$ data taken from de la Rosa et al. (2012). A strong statistically significant correlation (r= 0.97,

N= 19; p < 0.001) between LOI and $C_{org}$ was achieved, ensuring that LOI results are reflecting mostly $C_{org}$ (%OM).

In order to characterize OM quality, i.e. the percentages of labile and recalcitrant OM, the stepwise thermogravimetric procedure (STG) of Kristensen (1990) was applied to the cored samples from the Casa Branca salt marsh. According to this method, these OM fractions are defined as the percentage weight losses after ignition at 280ºC and 520ºC, respectively. In short, samples of 0.5 g were grounded and pre-dried at 105ºC for 6h. After cooling in a desiccator, the sample weight was determined with a precision of 0.1 mg. Next, the samples were combusted at precisely 280ºC for 6h in a computer controlled Heraeus MR 170 muffle furnace. After cooling in a desiccator and re-weighting, the samples returned to the muffle furnace and combusted at 520ºC for 6h. After cooling in a desiccator the final ash weight was determined (Kristensen, 1990).

**2.2. Solar activity, temperature, and precipitation climatic modelled data**

Cosmogenic radionuclides are produced in the atmosphere through a nuclear cascade mainly triggered by the high-energy galactic cosmic rays (GCR; Lal and Peters, 1967). As GCR enter the heliosphere, they are subject to modulation processes due to variable solar magnetic activity. This is the reason why during phases of low SA much higher particle intensities occur inside the heliosphere than during solar maximum conditions (e.g., Herbst et al., 2015; Adolphi and Muscheler, 2016). The two most noticeable cosmogenic radionuclides suitable for reconstructing SA are $^{14}C$ and $^{10}Be$. The production rate of both isotopes reacts in a very similar way to changes in solar and geomagnetic shielding (Masarik and Beer, 1999). The reconstructed dataset chosen for this work is the total solar irradiance (TSI), considered as a proxy for SA, from Steinhilber et al. (2012). This

268 reconstruction is based on time series of $^{14}$C stored in tree rings and of $^{10}$Be extracted from

269 polar ice cores, and was downloaded from the NOAA web page (http://www.noaa.gov/).

270 Aiming to compare the Br and OM records with climate variables, this study also

271 incorporates the series of temperature and precipitation evolution in both study areas as

272 predicted by a high-resolution regional climate model (Gómez-Navarro et al., 2011). The

273 simulation implements a domain that encompasses the whole Iberian Peninsula (IP) and

274 spans the second millennium entirely. It was carried out with a climate version of the

275 mesoscale model MM5, and driven at the boundaries by a simulation with the global model

276 ECHO-G (see Gómez-Navarro et al., 2011 for details). Following Gómez-Navarro et al.

277 (2011), the use of a high resolution model aims to reduce the scale gap between the large-

278 scale correctly simulated by the GCM and the features of regional variability present in the

279 Br and OM records presented here. The model simulates coherently the evolution of most

280 relevant climate variables, and in particular reproduces the physically constrained co-

281 evolution of temperature and precipitation, as well as their relation with large-scale

282 dynamics (e.g., the North Atlantic Oscillation – NAO). It is jointly driven by reconstructions of

283 the variability of three external forcings: TSI, greenhouse gas concentrations and the effect

284 of volcanic activity.

285

286 **2.3. Chronology**

287 The geochronology of the top 15 cm of the FWCBr core was calculated from the $^{210}$Pb

288 profile using the constant rate of supply method (CRS) (Appleby and Oldfield, 1978)

289 supported by $^{137}$Cs. Samples for $^{210}$Pb and $^{137}$Cs were analyzed following the methodology

290 described by Appleby (2001) at the University of Plymouth (UK) Consolidated Radioisotope

291 Facility, using an EG&G Ortec planar (GEM-FX8530-S N-type) HPGe gamma spectrometry

system built to ultra-low background specification for 210Pb detection. Additional information regarding the technique is provided in Appendix A. This core presented an unsupported $^{210}$Pb ($^{210}$Pbxs) profile that suggested some changes in the sediment accumulation rate in the upper section (*ca.* 150 years), although they could also reflect sediment mixing or disruption of the sedimentation. While the available elemental data is limited and presents generally low concentrations, the Pb profile shows slightly higher values above 18 cm that could be coincident with the initial stages of the industrial revolution (unclear date for this region but *ca.* AD 1800), which would be in agreement with the CRS model used here. However, the inflexion indicated by the model for the two older samples should be considered carefully (Leorri et al., 2010). In order to extend the chronology down-core, two samples (69–70 cm, 90–91 cm depth) of total organic carbon (TOC) were carbon-14 dated by accelerator mass spectrometry–AMS at Beta Analytic Inc. (USA). The chronology for the FWCBr core was created using a Bayesian age-depth model (Bchron 4.1; Haslett and Parnell, 2008; Parnell et al., 2008) (Appendix A). The model provides ages with an individual error for each sample averaging 73 years for a 95% confidence interval. The obtained calendar ages are presented in years of *Anno Domini* (years AD).

The chronology of the FCPw1 core can be found in Moreno et al. (2015), but also relies on the combination of $^{210}$Pb and carbon-14 data from TOC.


## 3. Results and discussion

### 3.1. Br⁻ in surface and interstitial water samples

The results of Br⁻ concentrations in surface and interstitial waters are presented in Table 1. Freshwater samples show Br⁻ contents between less than 0.01 mg/L (Minho River) and a

maximum of 0.8 mg/L (Sado River). On the other hand, marine surface water samples throughout the W coast have $Br^-$ contents ranging from 185 to 197 mg/L (Table 1). Such high values, outside the typical marine $[Br^-]$ range: 60–80 mg/L, are somewhat expected and connected or linked to the known supersaturation in brominated organic compounds in the Portuguese offshore (Raimund et al., 2011). This is related to the presence of strong macroalgal sources and to the Iberian Peninsula coastal upwelling, as discussed previously by Moreno et al. (2015). Brominated organic compounds (also including $CH_3Br$) are produced and degraded at relatively fast rates in the coastal ocean, with their degradation mechanisms (e.g., hydrolysis and chloride exchange reactions) in the water column as major suppliers of bromide anions to seawater. Our hypothesis – linking the $Br^-$ enrichment of western Portuguese superficial coastal waters to loss reactions of brominated organic compounds in seawater column – may be supported by other authors' findings. Namely, Hu et al. (2010) discovered for the east coast of United States evidence of a vertical distribution in the $CH_3Br$ saturation anomalies, with highest concentrations in the subsurface seawater below the mixed layer, due to high degradation rates near the surface. An analogous subsurface seawater enhancement in depth profiles of two of the most important short-lived carriers of atmospheric Br, i.e. dibromomethane ($CH_2Br_2$) and bromoform ($CHBr_3$), was described by Raimund et al. (2011) when sampling the Iberian Peninsula upwelling system off the coast of Portugal.

The detected $Br^-$ enrichment in the nearshore surface water samples also implies that marine water would have $Cl^-/Br^-$ mass ratios lower than the reported value for the average seawater (typically 290 ± 4; e.g., Katz et al., 2011). This chemical signature in our water samples is presented in the plot of $Cl^-/Br^-$ mass ratios versus $Cl^-$ in Figure 2, along with a typical marine water sample (TA_SW: $[Cl^-]$ = 19,353 mg/L and $[Br^-]$ = 67 mg/L; Millero, 2013). The clusters displayed by the $Cl^-/Br^-$ *vs.* $Cl^-$ plot allow to identify freshwater (with consistently lower levels of $Cl^-$ and $Br^-$) from marine and brackish waters reflecting an

14

increase in Cl⁻ (Figure 2A). In addition, it is possible to differentiate between the interstitial water samples of the NW coast salt marshes (Minho and Lima) and the SW coast samples (Sado and Mira) (Figure 2B). This suggests that beyond the inferred common main source of Br⁻ (and Cl⁻), i.e., seawater (theoretical ranges after Panno et al., 2006), a clear N–S differentiation can be established based on the relationship between the chemical indicators chloride and bromide. As shown in Figure 2B, the Sado and Mira interstitial waters, ranging from polyhaline (18–30‰) to euhaline (30–40‰), can be considered closer, based on these anions, to marine water samples (all clustering together; Figure 2B) than the ones from the Caminha and Lima salt marshes (mostly mesohaline: 5–18‰). These results are symptomatic of a stronger mixing with freshwater, originated by higher inputs of rainfall-land runoff production to the NW coast salt marshes, leading to salt dilution and lower ionic concentrations.

At this point, it must be emphasized that a rising body of evidence suggests that Br⁻ does not act conservatively in soils or water. Br⁻ can be (re)actively involved in OM cycling (e.g., Gerritse and George, 1988; Mahn and Gieskes, 2001; Biester et al., 2004, 2006; Leri et al., 2010, 2014), and it is frequently related to Fe and Mn cycling (e.g., Leri et al. 2010). This could diminish the "sensitivity" of the ratio Cl⁻/Br⁻, and limits its applicability as an inorganic tracer of marine intrusion. However, plotting Cl⁻/Br⁻ ratios provides insight into the Br⁻ (and Cl⁻) major sources in the sampled salt marshes. Panno et al. (2006) proposed Cl⁻/Br⁻ fingerprinting as a valuable diagnostic method in the identification of anthropogenic sources of salinization; though additional analysis should be required to complement this technique, and thus determine more accurately the source of the contaminant present in water samples. For instance, Figure 2B depicts a group of samples that evidence an anthropogenic impact based on this methodology – NSR_P1 (tidal flat; Lima), TRO_P7 (high marsh zone; Sado) and PMF_P6 (high marsh zone; Mira). The three fit in the "basin brines and animal waste" water-type (Panno et al., 2006). In addition, the sample TRO_P7

368 presents a measurable [$NO_3^-$] of 54 mg/L, by opposition to the other two, both with [$NO_3^-$] <

369 0.01 mg/L (results not shown). Historical Br anthropogenic sources such as emissions from

370 an antiknock additive in leaded gasoline, flame retardants, dyes, pharmaceuticals or

371 pesticides in agriculture are well-known (e.g., Flury and Papritz 1993), and while some were

372 phased out, others are still in use (e.g., Shaw et al., 2010). As briefly pointed in Section 2,

373 the Lima, Sado and Mira estuaries have their specific histories of anthropogenic

374 disturbances, but the effort to better distinguish the likely detected $Br^-$ contamination in

375 water samples (Figure 2B) is beyond the scope of the present study.

376

### 3.2. Br–OM relationships in marsh surface environments

378 The data gathered in the newly investigated salt marshes regarding interstitial waters (Table

379 1) are scarce due to several sampling and analytical constraints. This, together with the

380 presence of samples disturbed by anthropogenic activities frustrated our goal of broadening

381 the "evidence base" for natural [$Br^-$] interstitial water patterns in salt marshes. It was earlier

382 detected in the Caminha salt marsh that a pattern appears to be mainly dictated by marine

383 influence (periodic tidal flooding), i.e., higher [$Br^-$] in low marsh zone (average 71 mg/L;

384 Table 1), exposed to longer inundation periods by seawater and, consequently, prone to

385 greater inflow of bromide (Moreno et al., 2015). This is correlated with the relative

386 submersion times (annual basis) in the Caminha salt marsh, which is *ca.* 76–53% for tidal

387 flat, *ca.* 53–10% for low marsh and *ca.* 10–2% for the high marsh (Fatela et al., 2009).

388 $Br^-$ entering salt marshes can be cycled by several biotic and abiotic OM bromination

389 mechanisms (e.g., Keppler et al., 2000, 2004; Hamilton, 2003; Saito and Yokouchi, 2006;

390 Wishkerman et al., 2008; Leri et al., 2010; Leri and Myneni, 2012; Leri and Ravel, 2015). All

391 include the production of an oxidized form of Br that reacts with electron-rich organic

16

molecules, with the subsequent formation of organobromine by-products (Leri et al., 2014). Among them, it is the highly volatile gas $CH_3Br$ (e.g., Wuosmaa and Hager, 1990; Hamilton et al., 2003; Keppler et al., 2000, 2004; Saito and Yokouchi, 2006). Therefore, both the halophytic vegetation cover and the soil/sediment organic fraction of tidal salt marshes are the main settings and substrates for the conversion of inorganic Br ($Br_{inorg}$) into organic Br ($Br_{org}$), which can largely contribute to their Br pool (Moreno et al., 2015). It also explains why the total [Br] in (coastal) soils/sediments might not necessarily correlate with [$Br^-$] in water (Leri and Ravel, 2015). This lack of correlation is clear in the investigated salt marshes, where some mismatch is observed between [$Br^-$] in interstitial waters and the total [Br] gradient in surface soils/sediments (Tables 1 and 2; Figure 3). The highest total Br concentrations were found in the high marsh zones from Minho (average: 389 mg/kg) and Mira (avg.: 233 mg/kg) estuaries, while in their respective low marshes these contents did not exceed, on average, 133 mg/kg and 152 mg/kg (Table 2). Salt marshes from the Sado are the most depleted in both Br and OM, with average (median) values of 53 mg/kg and 8.2% (low marsh), and 81 mg/kg and 11.7% (high marsh), respectively. In the Lima estuary, Br trends are quite distinct (Table 2). This might be explained by the dominance of a coarser soil/sediment fraction (mainly sands) in the samples from these salt marshes transects (results not shown). Since a direct correlation has been well-established and widely accepted between mud (clay and/or silt) grain size fractions and both Br (e.g., Correns, 1956; Vinogradov, 1959) and OM (e.g., Buchanan and Longbottom, 1970; Mayer, 1994) contents, Br concentrations can be diluted in coarse-grained samples. The NSR_L transect is additionally impacted by a dredged sand processing facility located in the marsh surrounding area, causing resuspension of large quantities of sediment and disturbing this salt marsh (Cardoso et al., 2008).

The spatial pattern across soil/sediment surface transects (Figure 3) presents a strong direct correlation between Br and %OM (Lima: r= 0.89; N= 28; p < 0.001; Minho: r= 0.86;

418   N= 21; p < 0.001; Mira: r= 0.79; N= 29; p < 0.001, and Sado r= 0.67; N= 34; p < 0.001; tidal

419   flat samples are also included in the computed correlation coefficients). These results are in

420   good agreement with other studies (e.g., Cundy et al., 2005), suggesting that elevation is a

421   key factor controlling the soil/sediment $C_{org}$ pools of tidal salt marshes, as suggested by

422   Spohn and Giani (2012, 2013). These authors not only have found higher $C_{org}$ stocks in the

423   high marsh zones with limited flooding, but a major contribution of autochthonous (in situ)

424   OM inputs of the halophytic plant cover to soils and sediments at higher elevation within the

425   tidal frame. Such findings could likewise enlighten the preferential total Br enrichment in the

426   surface soils/sediments from the studied high marshes. Assuming that this Br is present

427   mainly as organobromine, the higher concentrations found in the high marsh zones,

428   typically characterized by greater density of stems and litter, can be associated to the

429   relatively fast oxidation of part of $Br^-$, which seems to lead to a rapid conversion to $Br_{org}$

430   (Leri and Myneni, 2012).

431   Similarly, the role of vegetation should be highlighted. The ubiquity of non-succulent

432   perennial species (*Juncus maritimus*) in the Caminha and Lima salt marshes contrasts with

433   the dominance of succulent species (e.g., from *Sarcocornia*/*Salicornia* genera) in Sado and

434   Mira salt marshes. Manley et al. (2006) and Blei et al. (2010) found higher relative Br

435   contents in succulent species, which (succulence) results from their strategy to survive in

436   saline soils by maintaining a large amount of tissue water. According to Manley et al.

437   (2006), high Br tissue levels would make of these succulent halophytes prolific $CH_3Br$

438   producers, although suggesting that each plant species has very different intrinsic abilities

439   to produce $CH_3Br$. Blei et al. (2010) showed that the variations in the Br content found on

440   salt marsh vegetation do not explain the spatial differences in $CH_3Br$ flux magnitudes,

441   concluding instead that the limiting factor lies on the plants conversion mechanism (abiotic

442   and/or biotic). Wishkerman et al. (2008) reported that the abiotic reaction (occurring

443   between plant pectin and Br followed by $CH_3Br$ emission) is strongly influenced by both air

temperatures, increasing by a factor of two for every 5ºC increase, and plants succulence, becoming more efficient as plants dry out. Rhew et al. (2014) estimated that only approximately 0.17% Br in the leaf tissue of *Batis maritima* L. (known as one of the $CH_3Br$ greatest producers in salt marshes) is daily removed via $CH_3Br$ emissions, indicating that to impact Br availability, a small separated subset of "*active* Br" at the enzyme site would be needed. According to them, if this *active* Br pool was 0.5% of the overall tissue content, then $CH_3Br$ emissions could reduce daily that pool by 34% for Br. This ongoing discussion is of major importance as it holds the power for unbalancing the total $[Br^-]$ (either reducing or increased it) available to ultimately be converted in $Br_{org}$ in a given marsh. As a final remark we would like to draw attention to the extensive intertidal habitat of *Zostera noltii* in Sado and Mira estuaries (Cunha et al., 2013), and its possible impact on the Br estuarine cycling. This seagrass along with *Zostera marina* Linnaeus 1753, which though very rare occurs as well in the Mira estuary (Cunha et al., 2013), also have been identified as producers/emitters of volatile Br compounds, such as $CH_3Br$ and $CHBr_3$ (Weinberg et al., 2013, 2015).

Interestingly, maximum Br soil/sediment enrichment in all studied salt marshes occurs in the highest low marsh transitioning to high marsh, in the so-called upper driftline zone (Adam, 1990; Gerlach 1999; Persicke et al. 1999; Lefeuvre et al., 2000; Gettner, 2003). These areas represent a tidal-terrestrial/freshwater transition interface, where most drift litter accumulates, usually containing a high concentration of seeds and vegetative material (Mineke and Bakker 2002). While this litter is effectively taken out of the estuarine circulation (e.g., Boorman, 2003), it becomes potentially accessible for promoting the magnification of the local $C_{org}$ pool of soils/sediments. As a result, and even if the understanding of the internal marsh processes affecting OM accumulation and turnover is limited (Fagherazzi et al., 2013) – identical to the mechanisms regulating $Br^-$ fluxes –, it seems plausible to consider the upper driftline zones as promising $Br_{org}$ sink areas, from the

standpoint of the current knowledge about OM bromination. Driftline zones might also be natural laboratories for studying the short and longer-term impacts of counterbalancing controls, like temperature, moisture and inundation (e.g., Lewis et al., 2014) as well as priming (e.g., Gontikaki et al., 2013) on OM mineralization, distressing Br sequestration and its fate in coastal environments.

Finally, the identified Br reduction in the soils/sediments collected at the highest high marsh (Figure 3) can be attributed to the increased influence of adjacent terrestrial uplands, taking into account the principle that the terrestrial environment, and thus terrestrial OM, is relatively poor in bromine (Mayer et al., 2007).

**3.2. Br temporal trends in SW (Mira estuary) and NW (Minho estuary) coasts**

*3.2.1. Comparing Br enrichment in relation to the long-term OM storage ability from salt marshes in their soils/sediments*

Casa Branca salt marsh (FWCBr core; Mira estuary) down-core profiles of Br and OM up to 89 cm depth (AD 1190) are presented in Figure 4, along with the profiles previously obtained from the Caminha salt marsh up to 62 cm depth (AD 1143) (FCPw1 core; Fig. 3 of Moreno et al., 2015). Also shown in Figure 4 are the corresponding computed Br/OM ratio trends for both cores.

The FWCBr core presents Br concentrations in the range 129–560 mg/kg while the OM content varies between 4.9% and 23.6% (Appendix B), with values uniform from the base (AD 1190) until around AD 1920 (Br: 129–215 mg/kg; average 161 ± 5 mg/kg; OM: 4.9–8.3%; average 6.7 ± 0.2%). Then, in the core's uppermost part, both Br and OM increase significantly, with two peaks at AD 1984 and AD 2010. This depth profile contrasts with the wider range and higher average Br content recorded in the FCPw1 core (Caminha):

average concentration of 747 mg/kg after the tidal marsh set up in AD 1330; minimum of 68 mg/kg, AD 1143 and maximum of 1300 mg/kg by AD 1700 (Moreno et al., 2015). It seems important to mention the concomitant tidal marsh build-up in both places, as indicated by the core's analysis of preserved benthic foraminifera associations: AD 1330 in Caminha (Moreno et al., 2014) and AD 1323 in Casa Branca (unpublished data). This event occurs during the transition from the Medieval Climatic Anomaly (MCA; 900–1300) to the LIA (1350–1900) and it is likely related to the main MCA–LIA shifts in local-to-regional hydroclimatic conditions in Iberian Peninsula (e.g., Lebreiro et al., 2006; Moreno et al., 2012).

The strong direct Br–OM correlation identified in surface marsh environments is preserved in the cored sediment samples with depth (r= 0.91; N= 30; p < 0.001), like previously described for the Caminha salt marsh (r= 0.83; N= 49; p < 0.001). This Br–OM correlation occurs independently of the large differences observed between the two cores regarding their Br and OM inventories (Figure 4). Indeed, and despite the evidence provided herein showing that the Mira estuary is subject to greater influence from $Br^-$ enriched coastal waters than Minho, the FWCBr core is relatively depleted in total Br (Appendix B). This depletion is also true for the amounts of long-term OM storage in both salt marshes soils/sediments. While in the FCPw1 core near 45% of the samples can be labelled as highly organic (OM > 30%) and *ca.* 41% as organic (organic content in the 15%–30% range), in the FWCBr core almost 94% of the samples can be classified as mineral soils with organics (organic content > 3% and ≤ to 15%) (Huang et al., 2009). Therefore, and consistent with the Br–OM relationship (leading to the production of organobromine compounds) found in the surface/modern marsh habitats, it can be hypothesized that the primary driver of the whole dissimilar Br pool size of these two coastal tidal marshes is their technical $C_{org}$ sink capacity, constraining the amount of $C_{org}$ that is sequestered in each. Generally, decomposition rates in salt marshes are lower than OM inputs (allochthonous

520 and autochthonous), the reason why they are recognized as one of the most powerful $C_{org}$

521 sinks on the planet (e.g., Macreadie et al., 2013). However, it is expected that at a regional

522 scale, soil/sediment $C_{org}$ pools are dependent upon several decomposition rate modifiers

523 (e.g., litter chemical composition, climate, nutrient availability, communities of soil/sediment

524 organisms, and site-specific factors), creating diverse geographic patterns as regards $C_{org}$

525 sequestration. Among those controls, salinity seems to be a major factor, and it is

526 suggested that on tidal marshes soil $C_{org}$ sequestration increases with decreasing salinity

527 (e.g., Poffenbarger et al., 2011; Van de Broek et al., 2016). Actually, salinity seems to have

528 an even stronger impact than elevation on the soil/sediment OM pools of tidal marshes,

529 inhibiting above-ground biomass and by enhancing OM mineralization (Hansen, 2015). In

530 the climatic context of the Mira estuary, the evapotranspiration rates usually exceed

531 precipitation, with tidal seawater supplying most of the moisture to the Casa Branca salt

532 marsh soils/sediments. This induces high salinity even on the high marsh (Table 1), with

533 Fatela et al. (2016) referring the occurrence of modern hypersaline conditions, with maxima

534 records of 48‰, in the Mira lower estuary. Foraminiferal evidence (that will be discussed

535 elsewhere) supports the idea that the (higher) Mira salinity baseline has been dominant

536 across the timeframe investigated, with assemblages dominated by *Jadammina*

537 *macrescens* (Brady, 1870) and *Trochammina inflata* (Montagu, 1808) (average 92%)

538 (unpublished data). Such high salinity baseline is, in turn, a possible explanation to the

539 lower OM in-depth concentrations from the FWCBr profile, which agrees with results from

540 other studies (e.g., Van de Broek et al., 2016 and references therein).

541 Moreover, climate has a fundamental influence on the quantity (and quality) of inputs to the

542 soil OM pool, with $C_{org}$ stocks being largest toward cooler and wetter locations, and smallest

543 at hotter and drier regions, as established by other studies of terrestrial ecosystems (e.g.,

544 Jenny, 1941; Meentemeyer, 1978; Liu et al., 2012, and references therein). These climatic

545 gradients can have left their signature on the temporal evolution of the $C_{org}$ storage in the

Caminha and Casa Branca study sites. This is revealed by their individual temporal soil/sediment OM patterns, developed in response to the long-term climatic gradient between the NW and SW coasts of rising temperature and decreasing precipitation (as can be observed in Figure 4), with plausible direct implications on Br longer-time-scale trend, as explained before.

The strong direct Br–OM correlation holds for both the labile (r= 0.92, N= 30; p < 0.001) and the relatively more recalcitrant OM (r= 0.88; N= 30; p < 0.001) fractions from the Casa Branca salt marsh soils/sediments (results not shown). This result is consistent with recent investigation, in which a series of model experiments allowed to establish the existence of a natural, abiotic mechanistic source both of aliphatic (more labile) and aromatic (more recalcitrant) forms of $Br_{org}$ in plant debris and humic substances in soil environment (Leri et al., 2014), and marine particulate OM (Leri and Ravel, 2015). The soil humic substances showed a recalcitrant aromatic $Br_{org}$ speciation, leading Leri et al. (2014) to suggest that this might provide a useful proxy for evaluating the rate of OM burial in sediments. In this direction, is worth mentioning the work by Biester et al. (2004, 2006) and Martínez-Cortizas et al. (2007, 2016) in peatland soils, where they have started to study the temporal trends of the more stable $Br_{org}$ compounds and the role of the main pedogenetic processes on Br accumulation. Altogether, this analysis can help future research on the Br–OM link in tidal marshes, needed to support the use of Br in marsh soils/sediments as a paleoclimatic indicator.

Finally, we propose a conceptual model for the salt marshes Br cycle in our case study (Caminha and Casa Branca) in order to summarize the interplay between the forcing factors analysed along the lines of the previous discussion. The interactions illustrated in Figure 5 are, in our view, the most likely to have a strong influence on salt marshes short and even longer-term role to act as a source and/or as a sink for Br. Accordingly, NW coast high

marshes under the sustained influence of concomitant lower photosynthetically active radiation (PAR), corresponding to the spectral range of solar radiation from 400 to 700 nm that is used in photosynthesis reactions (e.g., Mariscal et al., 2000), and colder wetter conditions developed lower salinity baselines where the vegetation cover largely consists of non-succulents. These lower salinity (mesohaline) tidal marshes have typically higher rates of plant productivity and lower decomposition rates of dead and senescing plant material, leading to higher accumulation of soil/sediment OM (e.g., Morrisey et al., 2014). Collectively, these processes culminate in lesser $CH_3Br$ atmospheric emissions from marshes and higher $Br_{org}$ concentration in their soils/sediments. On the other hand, the SW coast high marshes, settled under higher available PAR conditions and a hotter and dryer climate, show a higher (polyhaline to euhaline) salinity baselines and consequently lower productivity, being mostly colonized by succulent plants more adapted to saline conditions and greater emitters of $CH_3Br$. These conditions finally lead to a lower long-term storage of OM and $Br_{org}$ in soils/sediments.

The afore-described model establishes a connection with the analysis of the Br temporal variability in light of the past SA–climate link made in the next section.

*3.2.2. Br enrichment peaks in association with Grand Minima of solar activity*

The manifestation of a solar activity (SA) Grand Minima in terrestrial climate has been well established after the pioneering work of Eddy (1976). The most recent Grand Minima in reconstructed SA, as expressed by the TSI variation (Steinhilber et al., 2012), are presented in Figure 4 (Maunder Minimum – MM; 1645–1715; Spörer Minimum – SM; 1450–1550; and Wolf Minimum – WM; 1282–1342). Note that the Dalton Minimum (DM; 1790–1820) has a

distinct physical origin (Duhau and de Jager (2010), and it is therefore not regarded today as a Grand Episode of SA.

In the last few decades, extensive research work has been done towards a better understanding of the Sun-Earth's climate coupling system, with great progress being achieved (e.g., Haigh, 2007; Soon et al., 2014 for a review). Recently, Brugnara et al. (2013) referred that the Euro–Atlantic sector, in which Portugal is located, seems to be a region with a particularly strong solar influence on the troposphere, finding a weak but significant change in the mean late winter circulation over Europe, which culminates in detectable impacts on the near-surface climate. The results obtained by Jiang et al. (2015) suggest not only that climate in the northern North Atlantic regions follows SA fluctuations on multidecadal to centennial time scales, but also that it is more susceptible to the influence of those fluctuations throughout cool periods with, for instance, less vigorous ocean circulation. Similar results were found by Gómez-Navarro et al. (2012) in the context of climate simulations for the second millennium over the Iberian Peninsula. These researchers studied the impact of natural forcing and internal variability on climate, and found that temperature and precipitation variability are significantly affected at centennial scales by variations in the SA.

Grand Minima and Dalton-type Minimum scenarios are broadly characterized by (i) lower TSI (i.e., lower available PAR) (Lean, 1991, and references therein), (ii) development of cloudiness (e.g., Usoskin and Kovaltsov, 2008), and (iii) decreased global/regional air surface temperatures (e.g., Neukom et al., 2014) in tandem with greater regional precipitation variability. In the Iberian Peninsula, according with the modelled results from Gómez-Navarro et al. (2011), precipitation could have increased in response to reduced solar forcing (Figure 4), prompting greater river discharges. Also Cruz et al. (2015) related maxima rainfall episodes, as recognized in their stalagmite record, with other Grand Solar

Minima, suggesting a strong coupling between SA and precipitation over northern Iberia, which agrees with Gómez-Navarro et al. (2012) outcomes in the context of climate simulations.

Up to now, and in the absence of a "unified hypothesis", the explanations for the connections between solar phenomena and the lower atmosphere processes can be summarized in two types of mechanisms: (i) "top-to-down", influencing the pole-to-equator temperature gradient and exerting an impact on the modulation of the atmospheric circulation cells, weakening or strengthening the zonal winds, and (ii) "bottom-to-up" that directly impact on the radiation fluxes, energy balance and temperatures on the ground. Depending on the surface albedo a part of this radiation is absorbed and transformed into latent or sensible heat. During periods of lower SA, less radiation is available in the tropics for conversion to latent heat, which is thought to lead to a weakening of the Hadley and Ferrel cells (Labitzke et al., 2002). Other than intensity, the position and extent of those cells are also affected, inducing latitudinal shifts. Hence both mechanisms finally impact the atmospheric circulation modes responsible for the global/regional precipitation and temperature patterns (e.g., Gray et al., 2010; Martin-Puertas et al., 2012; Thiéblemont et al., 2015).

Therefore, if solar variations are an important source of regional climate variability, we might expect that paleoclimate proxies reproduce somewhat the climatic response to SA changes. In line with this, Moreno et al. (2015) suggested that Br soil/sediment enrichment in the Caminha salt marsh (NW coast) is, at least partially, related to the SA pattern over the last almost 800 years. This can be extended to Casa Branca salt marsh (SW coast), essentially through a SA control on (i) available PAR fluctuations and (ii) regional temperature and precipitation regimes, affecting evapotranspiration rates and, as a result, interstitial water salinity at the upper elevations within the marsh. Indeed, the relationship between the

curves presented in Figure 4 is clear, with periods of highest Br enrichment (FCPw1 and FWCBr) agreeing with major excursions in SA. This means that the TSI negative anomalies (Steinhilber et al., 2012) from the Dalton, Maunder, Spörer and Wolf Solar Minima, to which correspond periods of both modelled lower temperature and increased precipitation in the NW and SW of Portugal (Gómez-Navarro et al., 2011), are marked by Br positive peaks in marshes soils/sediments, more clearly observed in Br/OM ratio curves to account for changes in OM content (see black arrows). Considering only the group of samples from the FWCBr core falling within the LIA (with stronger impacts on the climate of Europe and other regions neighbouring the North Atlantic during the 16th–19th centuries; e.g., Mann, 2002), three display a more pronounced Br excess relative to OM, lying outside the upper 95% confidence limit of their linear regression interval: AD 1451 (Spörer Minimum), and AD 1694 and AD 1660 (both in the Maunder Minimum). These sedimentary records, considered altogether with other climatic proxies for the NW of Portugal (Moreno et al., submitted), strongly suggest that the LIA resulted in a wetter and cool climate in this south-western European region, triggering major hydrological changes present in paleoecological records, namely from high marsh benthic foraminifera (Moreno et al., 2014). Specifically, climatic shifts driven by Grand Minima on western Portuguese coast could have forced a deceleration of the whole dynamics involving the net $CH_3Br$ phytogenic emissions to the atmosphere, thus favouring Br sequestration and storage (as $Br_{org}$) in marsh soils/sediments. Throughout SA Grand Minima ($\downarrow$TSI/PAR), the climate controls departed from normal values ($\downarrow$T; $\downarrow$ET; $\uparrow$P; see Figure 5), inducing a decrease in marsh interstitial salinity, certainly ended in higher plant productivity peaks (e.g., De Leeuw et al., 1990), thereby causing a rise in salt marsh sediment $C_{org}$ accumulation over time, with plant debris more enriched in Br and liable to further bromination during the humification process.

Rhew et al. (2014) emphasized that $CH_3Br$ phytogenic emissions from coastal salt marshes, present a dramatic inter- and intra-marshes variability, namely in relation to magnitude

(subtropical salt marshes showing much higher emission rates than temperate salt marshes) and seasonality. They recorded maxima $CH_3Br$ emission fluxes in peak summer growing season (July) and lowest at the end of the growing season (November). The latter were registered during the morning and coincident with the high tide. They also found a pronounced mid-day peak, coinciding with the time of highest ambient air and surface soil temperatures, in the diurnal $CH_3Br$ emission trend, with this one mirroring the variation of PAR.

Considering both $CH_3Br$ phytogenic emissions and the ubiquity of soil/sediment OM bromination, and applying them to a Grand Minima scenario (↓TSI/available PAR; ↓air surface temperatures; ↓growing seasons, ↑rainfall leading to ↑soil/sediment saturation), a reliable framework for the Br enrichment in temperate marsh habitats triggered by climatic shifts driven by SA can be proposed (see Figure 5), recognizing that further work would be required to completely prove this assumption.

Volcanic eruptions may also represent an alternative source of Br to salt marshes during Grand Minima Episodes (see Figure 4). The first discovery of volcanic BrO (Bobrowski et al., 2003), and its subsequent measurement in many volcanic plumes around the globe (e.g., Roberts et al., 2014) demonstrates the formation of reactive bromine (firstly as $Br_2$, which then converts into other forms including Br, BrO, HOBr, $BrONO_2$) during these events, which can be removed (at least partially) from gaseous phase by aerosol, water and ice-uptake (followed by particle sedimentation) (Fernandez et al., 2014; Jourdain et al., 2015). Reactive bromine acts as a catalyst to its own formation, leading to an exponential growth called "bromine explosion". The LIA Grand Minima have been punctuated by considerable volcanic activity (e.g., D'Arrigo et al., 2013; Figure 4). D'Arrigo et al. (2013) highlighted, as two of the major volcanic events over the past millennium, the eruptions of AD 1453 (Kuwae Volcano, Vanuatu; Spörer Minimum) and AD 1815 (Mount Tambora,

695 Indonesia; Dalton Minimum). Such episodes of great volcanic activity and their worldwide

696 effects (e.g., Trigo et al., 2009; Koffman et al., 2013) might also have had the potential for

697 causing disruption on the Br cycling in Caminha and Casa Branca salt marshes, contributing

698 somewhat for their soils/sediments Br enrichment throughout Grand Minima.

699

## 4. Conclusions

701 The present study addresses major topics concerning the Br cycling in contrasting salt

702 marshes environments of four western Portuguese estuaries – Minho, Lima, Sado and Mira,

703 drawing attention for its complexity and linkages with OM dynamics. We provided evidence

704 that besides the marine influence, Br enrichment of these marshes is ultimately connected

705 to their ability for long-term $C_{org}$ storage. A clear difference between the marshes from NW

706 and SW coasts stands out, with the former being more enriched in both OM and total Br.

707 This contrasting behaviour is driven by different climatic conditions between the two regions

708 that favour more strongly the mechanisms and processes of OM production, burial, and

709 preservation (with concomitant incorporation of Br) in the north-western coastal salt

710 marshes, in contrast with the SW coast, most probably as a result of the higher salinity

711 (lesser productivity) of the latter. Seemingly, this same NW climatic setting inhibits the

712 emission of comparatively larger phytogenic $CH_3Br$ fluxes to atmosphere. This might be

713 intensified as a result of the marshes colonization by non-succulent species (less efficient in

714 the $CH_3Br$ production), further promoting the Br enrichment of soil/sediment OM.

715 Although the applied approach is constrained by chronological uncertainties, cores sampling

716 resolution or the (relatively short) time series lengths, preventing the application of

717 enhanced methodologies in the time-frequency domain, the Br temporal variability in the

718 Caminha and Casa Branca salt marshes can be related to SA oscillations, showing greater

29

Br enrichment during Grand Minima or Minima-like Episodes. This can be explained in connection with the changing temperature (decrease) and precipitation (increase) regimes in the NW and SW coasts of Portugal induced by lower TSI (available PAR), as pointed out by previous studies and supported by climate simulations. The contribution of major tropical volcanic explosions at Grand Solar Minima during the registered higher Br enrichment in the two Portuguese salt marshes is also considered.

Finally, we expect that the issues encompassed here can be deepened in future research about the Br biogeochemical cycle in salt marshes worldwide. The proposed conceptual framework identifies several influences capable of imbalance the Br–OM interconnections and helps to prioritize which are likely to play key roles on salt marshes Br recycling, in order to improve, henceforward, its reliability as a marker of climate change driven by past SA. In line with this, it is important to bear in mind that for robustly test solar-climate signals in Br tidal salt marsh records, large and widespread ensembles of well-dated data are required along with high-resolution sampling.

743

744 **References**

745

746 Adam, P., 1990. Salt marsh ecology. Cambridge University Press, Cambridge, UK, 461p.

747

748 Adams, S.S., 1969. Bromine in the Salado Formation, Carlsbad Potash District, New
749 Mexico. State Bureau of Mines and Mineral Resources, Bulletin 93, Socorro, New Mexico,
750 122 p.

751

752 Adolphi, F. and Muscheler, R., 2016. Synchronizing the Greenland ice core and radiocarbon
753 timescales over the Holocene – Bayesian wiggle-matching of cosmogenic radionuclide
754 records. Climate of the Past 12, 15–30.

755

756 Alcalá, F.J. and Custodio, E., 2008. Using the Cl/Br ratio as a tracer to identify the origin of
757 salinity in aquifers in Spain and Portugal; Journal of Hydrology 359, 189–207.

758

759 Almeida, C.M.R., Mucha, A.P. and Vasconcelos, M.T., 2011. Role of different salt marsh
760 plants on metal retention in an urban estuary (Lima estuary, NW Portugal). Estuarine,
761 Coastal and Shelf Science 91, 243–249.

762

763 Alves, A.M.C., 2003. O estuário do rio Lima: pressão antrópica e caracterização ambiental.
764 Ciências da Terra (UNL), Lisboa, special nº. V, CD-ROM, pp. H5–H9.

765

766 Amaral, V., Queiroga, H., Skov, M. and Paula, J., 2007. Planktonic availability and
767 settlement of *Carcinus maenas* megalopae at high temporal resolution in the lower Mira
768 Estuary (SW Portugal). Marine Ecology Progress Series 348, 239–248.

769

770 APA, 2011. Sistema Nacional de Informação de Ambiente da Agência Portuguesa do

771 Ambiente (SNIAmb).http://sniamb.apambiente.pt/.

772

773 Appleby, P.G., 2001. Chronostratigraphic techniques in recent sediments. *In* W.M. Last, J.P.

774 Smol (Eds.), Tracking Environmental Change Using Lake Sediments, 1. Dordrecht, The

775 Netherlands: Kluwer Academic Publishers, p. 171–203.

776

777 Appleby, P.G. and Oldfield, F., 1978. The calculation of lead-210 dates assuming a constant

778 rate of supply of unsupported $^{210}$Pb to the sediment. Catena 5, 1–8.

779

780 Araújo, M.F., Valério, P. and Jouanneau, J-M., 1998. Heavy metal assessment in sediments

781 of the Ave river basin (Portugal) by EDXRF. X-Ray Spectrometry 27, 305–312.

782

783 Araújo, M.F., Conceição, A., Barbosa, T., Lopes, M.T. and Humanes, H. 2003. Elemental

784 composition of marine sponges from the Berlengas Natural Park, Western Portuguese

785 Coast. X-Ray Spectrometry 32, 428–433.

786

787 Azevedo, I., Ramos, S., Mucha, A.P. and Bordalo, A.A., 2013. Applicability of ecological

788 assessment tools for management decision-making: A case study from the Lima estuary

789 (NW of Portugal). Ocean & Coastal Management 72, 54–63.

790

791 Bettencourt, A., Ramos, L., Gomes, V., Dias, J.M.A., Ferreira, G., Silva, M. and Costa, L.,

792 2003. Estuários Portugueses. Ed. INAG – Ministério das Cidades, Ordenamento do

793 Território e Ambiente, Lisboa, 311 p.

794

795   Biester, H., Keppler, F., Putschew, A., Martínez-Cortizas and Petri, M., 2004. Halogen

796   retention, organohalogens, and the role of organic matter decomposition on halogen

797   enrichment in two Chilean peat bogs. Environmental Science & Technology 38, 1984–1991.

798

799   Biester, H., Selimović, D., Hemmerich, S., and Petri, M., 2006. Halogens in pore water of

800   peat bogs – the role of peat decomposition and dissolved organic matter. Biogeosciences 3,

801   53–64.

802

803   Blei, E., Heal, M.R. and Heal, K.V., 2010. Long-term $CH_3Br$ and $CH_3Cl$ flux measurements

804   in temperate salt marshes. Biogeosciences 7, 3657–3668.

805

806   Bobrowski, N., Hönninger, G., Galle, B. and Platt, U., 2003. Detection of bromine monoxide

807   in a volcanic plume, Nature, 423, 273–276.

808

809   Boorman, L.A., 2003. Saltmarsh Review. An overview of coastal saltmarshes, their dynamic

810   and sensitivity characteristics for conservation and management. JNCC Report, No. 334,

811   113p.

812

813   Bridgham, S.D., Megonigal, J.P., Keller, J.K., Bliss, N.B. and Trettin, C., 2006. The carbon

814   balance of North American wetlands. Wetlands 26, 889–916.

815

816   Brugnara, Y., Brönnimann, S., Luterbacher, J. and Rozanov, E., 2013. Influence of the

817   sunspot cycle on the Northern Hemisphere wintertime circulation from long upper-air data

818   sets. Atmospheric Chemistry and Physics 13, 6275–6288.

819

820 Buchanan, J.B. and Longbottom, M.R., 1970. The determination of organic matter in marine

821 muds: the effect of the presence of coal and the routine determination of protein. Journal of

822 Experimental Marine Biology and Ecology 5, 158–169.

823

824 Cardoso, R., Araújo, M.F., Freitas, M.C. and Fatela, F., 2008. Geochemical characterisation

825 of sediments from marginal environments of Lima Estuary (NW Portugal). e-Terra, Revista

826 Electrónica de Ciências da Terra Volume 5 – Nº 6, GEOTIC – Sociedade Geológica de

827 Portugal, 11 p.

828

829 Carpenter, L.J. and Reimann, S. (Lead Authors), Burkholder, J.B., Clerbaux, C., Hall, B.D.,

830 Hossaini, R., Laube, J.C., and Yvon Lewis, S.A., 2014. Ozone-Depleting Substances

831 (ODSs) and Other Gases of Interest to the Montreal Protocol. Chapter 1 in Scientific

832 Assessment of Ozone Depletion: 2014, Global Ozone Research and Monitoring Project-

833 Report Nº 55, World Meteorological Organization, Geneva, Switzerland.

834

835 Castro, P. and Freitas, H., 2006. Anthropogenic effects and salt marsh loss in the Mondego

836 and Mira estuaries (Portugal). Web Ecology 6, 59–66.

837

838 Chipperfield, M.P., 2015. Global Atmosphere – The Antarctic Ozone Hole. *In* Still Only One

839 Earth: Progress in the 40 Years since the First UN Conference on the Environment, 2015,

840 pp. 1–33.

841

842 Correns, C.W., 1956. The Geochemistry of Halogens. *In* L.H. Ahrens, K. Rankama and S.K.

843 Rancorn (Eds.), Physics and Chemistry of the Earth, Vol. 1, Pergamon Press, New York,

844 pp. 181–233.

845

846 Costa, M.J. Catarino, F. and Bettencourt, A., 2001. The role of salt marshes in the Mira

847 estuary (Portugal). Wetlands Ecology and Management 9, 121–134.

848

849 Costa, J.C., 2001. Tipos de vegetação e adaptações das plantas do litoral de Portugal

850 continental. *In* M.E. Albergaria Moreira, A. Casal Moura, H.M. Granja and F. Noronha (Eds.)

851 Homenagem (in honorio) Professor Doutor Soares de Carvalho. Universidade do Minho,

852 Braga, pp. 283–299.

853

854 Costa, J.C., Arsénio, P., Monteiro-Henriques, T., Neto, C., Pereira, E., Almeida, T. and Izco,

855 J., 2009. Finding the boundary between Eurosiberian and Mediterranean salt marshes.

856 Journal of Coastal Research SI 56, 1340–1344.

857

858 Costa-Dias, S., Ronaldo Sousa, R. and Antunes, C., 2010. Ecological quality assessment of

859 the lower Lima Estuary. Marine Pollution Bulletin 61, 234–239.

860

861 Cox, M.L., Fraser, P.J., Sturrock, G.A., Siems, S.T. and Porter, L.W., 2004 Terrestrial

862 sources and sinks of halomethanes near Cape Grim, Tasmania. Atmospheric Environment

863 38, 3839–3852.

864

865 Crowley, T.J., 2000. Causes of climate change over the past 1000 years. Science 289,

866 270–277.

867

868 Cruz, J.A., Turrero, M.J., Cáceres, J.O., Marín-Roldán, A., Ortega, A.I., Garralón, A.,

869 Sánchez. L., Gómez, P., Munõz-García, M.B., Edwards, R.L. and J. Martín-Chivelet, J.,

870 2015. Long-term hydrological changes in northern Iberia (4.9–0.9 ky BP) from speleothem

Mg/Ca ratios and cave monitoring (Ojo Guarenã Karst Complex, Spain) Environmental Earth Sciences 74, 7741–7753.

Cundy, A.B., Hopkinson, L., Lafite, R., Spencer, K., Taylor, J.A., Ouddane, B., Heppell, C.M., Carey, P.J., Charman, R.O., Shell, D., Ullyott, J.S., 2005. Heavy metal distribution and accumulation in two Spartina sp.-dominated macrotidal salt marshes from the Seine estuary (France) and the Medway estuary (UK). Applied Geochemistry 20, 1195–1208.

Cunha, A.H., Assis, J.F. and Serrão, E.A., 2013. Seagrasses in Portugal: a most endangered marine habitat. Aquatic Botany 104, 193–203.

D'Arrigo, R., Wilson, R. and Anchukaitis, K.J., 2013. Volcanic cooling signal in tree ring temperature records for the past millennium. Journal of Geophysical Research: Atmospheres 118, 1–11.

De Leeuw, J., Olff, H. and Bakker, J.P., 1990. Year-to-year variation in peak above-ground biomass of six salt-marsh angiosperm communities as related to rainfall deficit and inundation frequency. Aquatic Botany 36, 139–151.

Dimmer, C.H., Simmonds, P.G., Nickless, G. and Nickless, M.R., 2000. Biogenic fluxes of halomethanes from Irish peatland ecosystems. Atmospheric Environment 35, 321–330.

Doff, D.H., 1989. Determination of bromine and iodine in four marine sediment reference samples by Energy-Dispersive X-Ray Fluorescence Spectrometry. Geostandards Newsletter 13, 75–77.

897 Drewer, J., Heal, M.R., Heal, K.V. and Smith, K.A., 2006. Temporal and spatial variation in
898 methyl halide flux from a salt marsh. Geophysical Research Letters 33, L16808, 5 p.

899

900 Duhau, S., and De Jager, C., 2010. The forthcoming Grand Minimum of solar activity,
901 Journal of Cosmology 8, 1983-1999.

902

903 Eddy, J.A., 1976. The Maunder Minimum. Science 192, 1189–1202.

904

905 Fagherazzi, S., Wiberg, P.L., Temmerman, S., Struyf, E., Zhao, Y. and Raymond, P.A.,
906 2013. Fluxes of water, sediments, and biogeochemical compounds in salt marshes.
907 Ecological Processes 2, 1–16.

908

909 Fatela, F., Moreno, J. and Cabral, M.C., 2016. Salinity and temperature water assessment
910 of the tidal marshes from the W Portuguese coast, as an ecological tool to
911 palaeoenvironmental reconstructions based on foraminifera and ostracoda assemblages.
912 Estudos do Quaternário, 14, http://www.apeq.pt/ojs/index.php/apeq.

913

914 Fatela, F., Moreno, J., Moreno, F., Araújo, M.F., Valente, T., Antunes, C., Taborda, R.,
915 Andrade, C., Drago, T., 2009. Environmental constraints of foraminiferal assemblages
916 distribution across a brackish tidal marsh (Caminha, NW Portugal). Marine
917 Micropaleontology 70, 70–88.

918

919 Fatela, F., Moreno, J. and Antunes, C., 2007. Salinity influence on foraminiferal tidal marsh
920 assemblages of NW Portugal: an anthropogenic constraint? Thalassas 23, 51–63.

921

Fernandez, R.P., Salawitch, R.J., Kinnison, D.E., Lamarque, J.-F. and Saiz-Lopez, A., 2014. Bromine partitioning in the tropical tropopause layer: implications for stratospheric injection. Atmospheric Chemistry and Physics 14, 13391–13410.

Ferreira, J.G., Simas, T., Nobre, A., Silva, M.C., Shifferegger, K. and Lencart-Silva, J., 2003. Identification of sensitive areas and vulnerable zones in transitional and coastal Portuguese systems. INAG, Lisboa, 151 p.

Flury, M. and Papritz, A., 1993. Bromide in the natural environment: occurrence and toxicity. Journal of Environmental Quality 22, 747–758.

Gerlach, A., 1999. Winter driftline debris on the Wadden Island of Mellum, Germany; distribution, quantity and decomposition. Abhandlungen Naturwissenschaftliches Verein Bremen 44, pp. 707–724.

Gerritse, R.G. and George, R., 1988. The role of soil organic matter in the geochemical cycling of chloride and bromide. Journal of Hydrology 101, 83–95.

Gettner, S., 2003. Untersuchungen des Zusammenhangs zwischen Treibselmengen und Vorlandnutzung an der Westküste Schleswig-Holsteins. Kieler Notizen Pflanzenkunde Schleswig Holstein Hamburg 31, pp. 57–71.

Gómez-Navarro, J.J., Montávez, J.P., Jiménez-Guerrero, P., Jerez, S., Lorente-Plazas, R., González-Rouco, J.F. and Zorita, E., 2012. Internal and external variability in regional simulations of the Iberian Peninsula climate over the last millennium. Climate of the Past 8, 25–36.

948

949 Gómez-Navarro, J.J., Montávez, J.P., Jerez, S., Jiménez-Guerrero, P., Lorente-Plazas, R.,

950 González-Rouco, J.F. and Zorita, E., 2011. A regional climate simulation over the Iberian

951 Peninsula for the last millennium. Climate of the Past 7, 451–472.

952

953 Gontikaki, E., Thornton, B., Huvenne, V.A.I. and Witte, U., 2013. Negative priming effect on

954 organic matter mineralisation in NE Atlantic slope Sediments. PLoS ONE 8(6): e67722, 9 p.

955

956 Gray, L.J, Beer, J., Geller, M., Haigh, J.D., Lockwood, M., Matthes, K., Cubasch, U.,

957 Fleitmann, D., Harrison, G., Hood, L., Luterbacher, J., Meehl, G.A., Shindell, D., van Geel,

958 B. and White, W. 2010. Solar influences on climate. Reviews of Geophysics 48, RG4001,

959 53 p.

960

961 Haigh, J.D., 2007. The sun and the earth's climate. Living Review Solar Physics 4, 1e64

962 (Online article). Available at: http://www.livingreviews.org/lrsp-2007-2 (accessed

963 08.05.2016).

964

965 Hamilton, J., McRoberts W., Keppler, F., Kalin, R. and Harper, D., 2003. Chloride

966 methylation by plant pectin: An efficient environmentally significant process, Science 301,

967 206–209.

968

969 Hansen, K., 2015. Ecosystem functions of tidal marsh soils of the Elbe estuary. Dissertation,

970 Fachbereich Geowissenschaften, Universität Hamburg, Hamburger Bodenkundliche

971 Arbeiten 76, XX + 161p.

972

973 Hardacre, C.J. and Heal, M.R., 2013. Characterization of methyl bromide and methyl

974 chloride fluxes at temperate freshwater wetlands. Journal of Geophysical Research:

975 Atmospheres 118, 977–991.

976

977 Hardacre, C.J., Blei, E. and Heal, M.R., 2009. Growing season methyl bromide and methyl

978 chloride fluxes at a sub-arctic wetland in Sweden. Geophysical Research Letters 36,

979 L12401, 5 p.

980

981 Haslett, J. and Parnell, A., 2008. A simple monotone process with application to

982 radiocarbon-dated depth chronologies. Applied Statistics 57, 399–418.

983

984 Herbst, K., Heber, B., Beer, J. and Tylka, A.T., 2015. Modelling the Production of

985 Cosmogenic Radionuclides due to galactic and solar cosmic rays. The 34th International

986 Cosmic Ray Conference, PoS (ICRC2015) 537, 8p.

987

988 Honrado, J., Alves, P., Alves, H.N., Torres, J. and Caldas, F.B., 2004. A Flora e a

989 vegetação do Minho internacional – Diversidade, ecologia e valor para conservação.

990 Melgaço, Portugal: Atas do Congresso Internacional Sobre o Rio Minho; 5p.

991

992 Hu, L., Yvon-Lewis, S.A., Liu, Y., Salisbury, J.E. and O'Hern, J.E., 2010. Coastal emissions

993 of methyl bromide and methyl chloride along the eastern Gulf of Mexico and the east coast

994 of the United States. Biogeochemical Cycles 24, GB1007, 10 p.

995

996 Huang, P.-T., Patel, M., Santagata, M.C., and Bobet, A., 2009. Classification of organic

997 soils. FHWA/IN/JTRP-2008/2. Purdue University, 170 p.

998

Hurrell, J., 1995. Decadal trends in the North-Atlantic Oscillation: regional temperatures and precipitation. Science 269, 676–679.

Hurrell, J. and van Loon, H., 1997. Decadal variations in climate associated with the North Atlantic Oscillation. Climatic Change 36, 301–336.

Jenny, H., 1941. Factors of Soil Formation - A System of Quantitative Pedology. Dover Publications, Inc., New York, 291 p.

Jiang, H., Muscheler, R., Björck, S., Seidenkrantz, M.-S., Olsen, J., Sha, L., Sjolte, J., Eiríksson, J., Ran, L., Knudsen, K.-L., and Knudsen, M.F., 2015. Solar forcing of Holocene summer sea-surface temperatures in the northern North Atlantic. Geology doi:10.1130/G36377.1.

Jones, F., Vengosh, A., Rosenthal, E., Yechieli, Y., 1999. Geochemical investigation of groundwater quality. In: Proceeding: Seawater Intrusion in Coastal Aquifers - Concepts, Methods and Practices. Kluwer Academic, Dordrecht, pp. 51–71.

Jourdain, L., Roberts, T.J., Pirre, M. and Josse, B., 2015. Modeling the reactive halogen plume from Ambrym volcano and its impact on the troposphere with the CCATT-BRAMS mesoscale model. Atmospheric Chemistry and Physics Discuss. 15, 35313–35381.

Katz, B.G., Eberts, S.M. and Kauffman, L.J., 2011. Using Cl/Br ratios and other indicators to assess potential impacts on groundwater quality from septic systems: A review and examples from principal aquifers in the United States. Journal of Hydrology 397, 151–166.

1025 Keene, W.C., Stutz, J., Pszenny, A.A.P., Maben, J.R., Fischer, E.V., Smith, A.M., von

1026 Glasow, R., Pechtl, S., Sive, B.C. and Varner, R.K., 2007. Inorganic chlorine and bromine in

1027 coastal New England air during summer. Journal of Geophysical Research 112, D10S12,

1028 15 p.

1029

1030 Keller, J.K., Bauers, A.K., Bridgham, S.D., Kellogg, L.E. and Iversen, C.M., 2006. Nutrient

1031 control of microbial carbon cycling along an ombrotrophic-minerotrophic peatland gradient,

1032 Journal of Geophysical Research 111, G03006, 14 p.

1033

1034 Keppler, F., Eiden, R., Niedan, V., Pracht, J., and Scholer, H.F., 2000. Halocarbons

1035 produced by natural oxidation processes during degradation of organic matter, Nature 403,

1036 298–301.

1037

1038 Keppler, F., Kalin, R.M., Harper, D.B., McRoberts, W.C. and Hamilton, J.T.G., 2004. Carbon

1039 isotope anomaly in the major plant C1 pool and its global biogeochemical implications,

1040 Biogeosciences 1, 123–131.

1041

1042 Koffman, B.G., Kreutz, K.J., Kurbatov, A.V. and Dunbar, N.W., 2013. Impact of known local

1043 and tropical volcanic eruptions of the past millennium on the WAIS Divide microparticle

1044 record. Geophysical Research Letters 40, 4712–4716.

1045

1046 Koh, D.-C., Mayer, B., Lee, K.-S. and Ko, K.-S., 2010. Land-use controls on sources and

1047 fate of nitrate in shallow groundwater of an agricultural area revealed by multiple

1048 environmental tracers. Journal of Contaminant Hydrology 118, 62–78.

1049

Kristensen, E., 1990. Characterization of biogenic organic matter by stepwise thermogravimetry (STG). Biogeochemistry 9, 135–159.

Labitzke, K., Austin, J., Butchardt, N., Knight, J., Takahashi, M., Nakamoto, M., Nagashima, T., Haigh, J., and Williams, V., 2002. The global signal of the 11-year solar cycle in the stratosphere: observations and models, Journal of Atmospheric and Solar-Terrestrial Physics 64, 203–210.

Lal, D. and Peters, B., 1967. Cosmic ray produced radioactivity on the Earth. *In* K. Sitte (Ed.), Handbuch der Physic / Encyclopedia of Physics, vol. 9 / 46 / 2, Springer-Verlag, Berlin, pp. 551–612.

Lean J., 1991. Variations in the sun's radiative output. Reviews of Geophysics 29, 505–535.

Lebreiro, S.M., Francés, S.G., Abrantes, F.F.G., Diz, P., Bartels-Jónsdóttir, H.B., Stroynowski, Z.N., Gil, I.M., Pena, L.D., Rodrigues, T., Jones, P.D., Nombela, M.A., Alejo, I., Briffa, K.R., Harris, I. and Grimalt, J.O., 2006. Climate change and coastal hydrographic response along the Atlantic Iberian margin (Tagus Prodelta and Muros Ría) during the last two millennia. The Holocene 16, 1003–1015.

Lefeuvre, J.-C., Bouchard, V., Feunteun, E., Grare, S., Laffaille, P. and Radureau, A., 2000. European salt marshes diversity and functioning: the case study of the Mont Saint-Michel bay, France. Wetland Ecology and Management 8, 147–161.

1074    Leorri, E., Freitas, M.C., Zourarah, B., Andrade, C., Mellas, S., Cruces, A., Griboulard, R.

1075    and Lopes, V., 2010. Multiproxy approach to characterize an overwash deposit: Oualidia

1076    lagoon (Moroccan Atlantic coast). GEOGACETA 48, 7–10.


1078    Leri, A.C. and Ravel, B., 2015. Abiotic bromination of soil organic matter. Environmental

1079    Science & Technology 49, 13350–13359.


1081    Leri, A.C., Mayer, L.M., Thornton, K.R. and Ravel, B., 2014. Bromination of marine

1082    particulate organic matter through oxidative mechanisms. Geochimica et Cosmochimica

1083    Acta 142, 53–63.


1085    Leri, A.C. and Myneni, S.C.B., 2012. Natural organobromine in terrestrial ecosystems.

1086    Geochimica and Cosmochimica Acta 77, 1–10.


1088    Leri, A.C., Hakala, J.A., Marcus, M.A., Lanzirotti, A., Reddy, C.M. and Myneni, S.C.B., 2010.

1089    Natural organobromine in marine sediments: new evidence of biogeochemical Br cycling.

1090    Global Biogeochemical Cycles 24, GB4017, 15 p.


1092    Lewis, D.B., Brown, J.A. and Jimenez, K.L., 2014. Effects of flooding and warming on soil

1093    organic matter mineralization in *Avicennia germinans* mangrove forests and *Juncus*

1094    *roemerianus* salt marshes. Estuarine, Coastal and Shelf Science 139, 11–19.


1096    Lima, I., Moreira, S.M., Osten, JR.-V., Soares, A.M.V.M. and Guilhermino, L., 2007.

1097    Biochemical responses of the marine mussel *Mytilus galloprovincialis* to petrochemical

1098    environmental contamination along the North-western coast of Portugal. Chemosphere 66,

1099    1230–1242.

Liu, Z.P., Shao, M.A. and Wang, Y.Q., 2012. Large-scale spatial variability and distribution of soil organic carbon across the entire Loess Plateau, China. Soil Research 50, 114–124.

Macreadie, P.I., Hughes, A.R. and Kimbro, D.L., 2013. Loss of "blue carbon" from coastal salt marshes following habitat disturbance. PLoS ONE 8, e69244, 8 p.

Mahn, C.L. and Gieskes J.M., 2001. Halide systematics in comparison with nutrient distributions in sites 1033B and 1034B, Saanich Inlet: ODP Leg 169S. Marine Geology 174, 323–339.

Manley, S.L., Wang, N.-Y., Walser, M.L., and Cicerone, R.J., 2006. Coastal salt marshes as global methyl halide sources from determinations of intrinsic production by marsh plants. Global Biogeochemical Cycles 20, GB3015, 13 p.

Mann, M.E., Zhang, Z., Rutherford, S., Bradley, R.S., Hughes, M.K., Shindell, D., Ammann, C., Faluvegi, G. and Ni, F., 2009. Global signatures of the Little Ice Age and Medieval climate anomaly and plausible dynamical origins, Science 326, 1256–1260.

Mayer, L.M., 1994. Relationships between mineral surfaces and organic carbon concentrations in soils and sediments. Chemical Geology 114, 347–363.

Mayer, L.M., Schick, L.L., Allison, M.A., Ruttenberg, K.C. and Bentley, S.J., 2007. Marine vs. terrigenous organic matter in Louisiana coastal sediments: The uses of bromine:organic carbon ratios. Marine Chemistry 107, 244–254.

1126 Mariscal, M.J., Orgaz, F. and Villalobos, F.J., 2000. Modelling and measurement of
1127 radiation interception by olive canopies. Agricultural and Forest Meteorology 100,183–197.

1128

1129 Marques, B., Lillebø A.I., Pereira, E. and Duarte, A.C., 2011. Mercury cycling and
1130 sequestration in salt marshes sediments: An ecosystem service provided by *Juncus*
1131 *maritimus* and *Scirpus maritimus*. Environmental Pollution 159, 1869–1876.

1132

1133 Martin-Puertas, C., Matthes, K., Brauer, A., Muscheler, R., Hansen, F., Petrick, C., Aldahan,
1134 A., Possnert, G. and van Geel, B., 2012. Regional atmospheric circulation shifts induced by
1135 a grand solar minimum. Nature Geoscience 5, 397–401.

1136

1137 Martínez-Cortizas, A., Vázquez, C.F., Kaal, J., Biester, H., Casais, M.C., Rodríguez, T.T.
1138 and Lado, L.R., 2016. Bromine accumulation in acidic black colluvial soils. Geochimica et
1139 Cosmochimica Acta 174, 143–155.

1140

1141 Martínez-Cortizas, A., Biester, H., Mighall, T. and Bindler, R., 2007. Climate-driven
1142 enrichment of pollutants in peatlands. Biogeosciences 4, 905–911.

1143

1144 Martins, F., Leitão, P., Silva, A. and Neves, R., 2001. 3D modelling in the Sado estuary
1145 using a new generic vertical discretization approach. Oceanologica Acta 24, 1–12.

1146

1147 Masarik, J. and Beer, J., 1999. Simulation of particle fluxes and cosmogenic nuclide
1148 production in the Earth's atmosphere. Journal of Geophysical Research 104, 12099–12111.

1149

1150 Meentemeyer, V., 1978. Macroclimate and lignin control of litter decomposition rates.
1151 Ecology 59, 465–472.

Millero, F.J., 2013. Chemical Oceanography, CRC Press, 4th edition, Boca Raton, 571 p.

Mineke, W. and Bakker, J.P., 2002. Soil seed bank and driftline composition along a successional gradient on a temperate salt marsh. Applied Vegetation Science 5, 55–62.

Moreira, M.E.S.A., 1992. Recent saltmarsh changes and sedimentation rates in the Sado estuary, Portugal. Journal of Coastal Research 8, 631–640.

Moreno, A., Pérez, A., Frigola, J., Nieto-Moreno, V., Rodrigo-Gámiz, M., González-Sampériz, P., Morellón, M., Martín-Puertas, C., Corella, J.P., Belmonte, Á., Sancho, C., Cacho, I., Herrera, G., Canals, M., Jiménez-Espejo, F., Martínez-Ruiz, F., Vegas, T. and Valero Garcés, B.L., 2012. The Medieval Climate Anomaly in the Iberian Peninsula reconstructed from marine and lake records. Quaternary Science Reviews 43, 16–32.

Moreno, J., Fatela, F., M.A. Gonçalves, M.A., Leorri, E., Gómez-Navarro, J.J., Brázdil, R., Ferreira, M.J., Moreno, F. and R. Trigo (submitted). A bi-proxy paleoclimatic reconstruction for the Entre-Douro-e-Minho region, northwest Portugal, from 1626 to 1820 – A search for evidence of solar forcing.

Moreno, J., Fatela, F., Leorri, E., Araújo, M.F., Moreno, F., De la Rosa, J.M., Freitas, M.C., Valente, T. and Corbett, R., 2015. Bromine enrichment in marsh sediments as a marker of environmental changes driven by Grand Solar Minima and Anthropogenic activity (Caminha, NW of Portugal). Science of the Total Environment 506–507, 554–566.

Moreno, J., Fatela, F., Leorri, E., De la Rosa, J., Pereira, I., Araújo, M.F., Freitas, M.C., Corbett, R. and Medeiros, A., 2014. Marsh benthic foraminifera response to estuarine hydrological balance driven by climate variability over the last 2000 years (Minho estuary, NW Portugal). Quaternary Research 82, 318–330.

Moreno, J., Fatela, F., Andrade, C., Cascalho, J., Moreno, F. and Drago, T., 2005. Living foraminiferal assemblages from the Minho and Coura estuaries (Northern Portugal): a stressful environment. Thalassas 21, 17–28.

Morrisey, E.M., Gillespie, J.L., Morina, J.C. and Franklin, R.B., 2014. Salinity affects microbial activity and soil organic matter content in tidal wetlands. Global Change Biology 20, 1351–1362.

Neubauer, S.C., Franklin, R.B. and Berrier, D.J., 2013. Saltwater intrusion into tidal freshwater marshes alters the biogeochemical processing of organic carbon Biogeosciences Discussions 10, 10685–10720.

Neukom, R. Gergis, J. 3, Karoly, D.J., Wanner, H., Curran, M., Elbert, J., González-Rouco, F., Linsley, B.K, Moy, A.D., Mundo, I.,10, Raible, C.C.,1,11, Steig, E.J., van Ommen, T., Vance, T. Villalba, R., Zinke, J. and Frank, D., 2014. Inter-hemispheric temperature variability over the past millennium. Nature Climate Change 4, 362–367.

Neuparth, T., Correia, A.D., Costa, F.O., Lima, G. and Costa, M.H., 2005. Multi-level assessment of chronic toxicity of estuarine sediments with the amphipod *Gammarus locusta*: I. Biochemical endpoints. Marine Environmental Research 60, 69–91.

Nittrouer, C.A., Sternberg, R.W., Carpenter, R. and Bennett, J.T., 1979. The use of $^{210}$Pb geochronology as a sedimentological tool: application to the Washington Continental Shelf. Marine Geology 31, 297–316.

Obrist, D., Tas, E., Peleg, M., Matveev, V., Faïn, X., Asaf, D. and Luria, M., 2011. Bromine-induced oxidation of mercury in the mid-latitude atmosphere. Nature Geoscience 4, 22–26.

Panno, S.V., Hackley, K.C., Hwang, H.H., Greenberg, S.E., Krapac, I.G., Landsberger, S. and O'Kelly, D.J., 2006. Characterization and identification of Na-Cl sources in ground water. Ground Water 44, 176–187.

Parnell, A., Haslett, J., Allen, J., Buck, C. and Huntley, B., 2008. A flexible approach to assessing synchronicity of past events using Bayesian reconstructions of sedimentation history. Quaternary Science Reviews 27, 1872–1885.

Paula, J., Silva, I.C., Francisco, S.M. and Flores, A.V., 2006. The use of artificial benthic collectors for assessment of spatial patterns of settlement of megalopae of *Carcinus maenas* (L.) (Brachyura: Portunidae) in the lower Mira Estuary, Portugal. Hydrobiologia 557, 69–77.

Persicke, U., Gerlach, A. and Heiber, W., 1999. Zur botanischen Zusammensetzung von Treibsel der niedersachsischen Deichvorlander und Deichabsnitte. Drosera 1, 23–34.

Poffenbarger, H.J., Needelman, B.A. and Megonigal, J.P., 2011. Salinity influence on methane emissions from tidal marshes. Wetlands 31, 831–842.

Raimund, S., Quack, B., Bozec, Y., Vernet, M., Rossi, V., Garçon, V., Morel, Y. and Morin P., 2011. Sources of short-lived bromocarbons in the Iberian upwelling system. Biogeosciences 8, 1551–1564.

Reis, P.A., Guilhermino. L., Antunes, C., and Sousa, R., 2014. Assessment of the ecological quality of the Minho estuary (Northwest Iberian Peninsula) based on metal concentrations in sediments and in *Corbicula fluminea*. Limnetica 33, 161–174.

Rhew, R.C., Whelan, M.E. and Min, D.-H., 2014. Large methyl halide emissions from south Texas saltmarshes. Biogeosciences 11, 6427–6434.

Rhew, R.C. and Mazéas, O., 2010. Gross production exceeds gross consumption of methyl halides in northern California salt marshes. Geophysical Research Letters 37, L18813, 5 p.

Rhew, R.C., Miller, B.R., Bill, M., Goldstein, A.H. and Weiss, R.F., 2002. Environmental and biological controls on methyl halide emissions from southern California coastal salt marshes. Biogeochemistry 60, 141–161.

Rhew, R.C., Miller, B.R. and Weiss, R.F., 2000. Natural methyl bromide and methyl chloride emissions from coastal salt marshes. Nature 403, 292–295.

Roberts, T.J., Martin, R.S. and Jourdain, L., 2014. Reactive bromine chemistry in Mount Etna's volcanic plume: the influence of total Br, high-temperature processing, aerosol loading and plume–air mixing. Atmospheric Chemistry and Physics 14, 11201–11219.

Saito, T. and Yokouchi, Y., 2006. Diurnal variation in methyl halide emission rates from tropical ferns. Atmospheric Environment 40, 2806–2811.

Shaw, S.D., Blum, A., Weber, R., Kannan, K., Rich, D., Lucas, D., Koshland, C.P., Dobraca, D., Hanson, S. and Birnbaum, L.S., 2010. Halogenated flame retardants: do the fire safety benefits justify the risks? Reviews on Environmental Health 25, 261–305.

Smith, J.N., 2001. Why should we believe $^{210}$Pb sediment geochronologies? Journal of Environmental Radioactivity 55, 121–123.

Soon, W., Velasco Herrera, V.M., Selvaraj, K., Traversi, R., Usoskin, I., Chen, C.-T.A., Lou, J.-Y., Kao, S.-J., Carter, R.M., Pipin, V., Severi, M. and Becagli, S., 2014. A review of Holocene solar-linked climatic variation on centennial to millennial timescales: physical processes, interpretative frameworks and a new multiple cross-wavelet transform algorithm. Earth Science Reviews 134, 1–15.

Spohn, M., Babka, B. and Giani, L., 2013. Changes in soil organic matter quality during sea-influenced marsh soil development at the North Sea coast. Catena 107, 110–117.

Spohn, M. and Giani, L., 2012. Carbohydrates, carbon and nitrogen in soils of a marine and a brackish marsh as influenced by inundation frequency. Estuarine, Coastal and Shelf Science 107, 89–96.

Steinhilber, F., Abreu, J.A., Beer, J., Brunner, I., Christl, M., Fischer, H., Heikkilä, U., Kubik, P.W., Mann, M., McCracken, K.G., Miller, H., Miyahara, H., Oerter, H. and Wilhelms, F.,

1281  2012. 9,400 years of cosmic radiation and solar activity from ice cores and tree rings.

1282  Proceedings of the National Academy of Sciences 109, 5967–5971.

1283

1284  Usoskin, I.G. and Kovaltsov, G.A., 2008. Cosmic rays and climate of Earth: Possible

1285  connection, Comptes Rendus Geoscience 340, 441–450.

1286

1287  Vale, L.M. and Dias, J.M., 2011. The effect of tidal regime and river flow on the

1288  hydrodynamics and salinity structure of the Lima Estuary: Use of a numerical model to

1289  assist on estuary classification, SI 64 (Proceedings of the 11th International Coastal

1290  Symposium), Szczecin, Poland, pp. 1604–1608.

1291

1292  Taborda, R., Dias, J.M.A., 1991. Análise da sobre-elevação do nível do mar de origem

1293  meteorológica durante os temporais de 1978 e 1981. Geonovas, SI 1, 89–97.

1294

1295  Thiéblemont, R., Matthes, K., Omrani, N.-E., Kodera, K. and Hansen, F., 2015. Solar forcing

1296  synchronizes decadal North Atlantic climate variability. Nature Communications 6:8268. 8 p.

1297

1298  Trigo, R.M., Vaquero, J.M., Alcoforado, M.J., Barriendos, M., Taborda, J., García-Herrera R.

1299  and Luterbacher, J., 2009. Iberia in 1816, the year without a summer. International Journal

1300  of Climatology 29, 99–115.

1301

1302  Van de Broek, M., Temmerman, S., Merckx, R. and Govers, G., 2016. The importance of an

1303  estuarine salinity gradient on soil organic carbon stocks of tidal marshes. Biogeosciences

1304  Discussions, doi:10.5194/bg-2016-285.

1305

1306 Varner, R.K., Crill, P.M. and Talbot, R.W., 1999. Wetlands: A potentially significant source

1307 of atmospheric methyl bromide and methyl chloride, Geophysical Research Letters 26,

1308 2433– 2435.

1309

1310 Vinogradov, A.P., 1959. The Geochemistry of Rare and Dispersed Elements in Soils.

1311 Second edition, Consultants Bureau, New York, 209 p.

1312

1313 Weinberg, I., Bahlmann, E., Eckhardt, T., Michaelis, W. and Seifert, R., 2015. A halocarbon

1314 survey from a seagrass dominated subtropical lagoon, Ria Formosa (Portugal): flux pattern

1315 and isotopic composition. Biogeosciences 12, 1697–1711.

1316

1317 Weinberg, I., Bahlmann, E., Michaelis, W. and Seifert, R., 2013. Determination of fluxes and

1318 isotopic composition of halocarbons from seagrass meadows using a dynamic flux

1319 chamber. Atmospheric Environment 73, 34–40.

1320

1321 Wishkerman, A., Gebhardt, S., McRoberts, C.W., Hamilton, J.T.G., Williams, J. and

1322 Keppler, F., 2008. Abiotic methyl bromide formation from vegetation and its strong

1323 dependence on temperature. Environmental Science & Technology 42, 6837–6842.

1324

1325 Wuosmaa, A. M. and Hager, L. P., 1990. Methyl chloride transferase: a carbocation route

1326 for biosynthesis of halometabolites, Science 249, 160–162.

1327

1328 Yvon-Lewis, S.A., Saltzman, E.S. and Montzka, S.A., 2009. Recent trends in atmospheric

1329 methyl bromide: analysis of post-Montreal Protocol variability. Atmospheric Chemistry and

1330 Physics 9, 5963–5974.

1331

1332 Ziegler, M., Jilbert, T., de Lange, G.J., Lourens L.J. and Reichart, G.-J., 2008. Bromine

1333 counts from XRF scanning as an estimate of the marine organic carbon content of sediment

1334 cores. Geochemistry Geophysics Geosystems 9, Q05009, 6 p.

1335

1336 http://www.icnf.pt/portal/ap/r-nat/rnet/geo

1337 http://www.noaa.gov/

1338

1339

1340
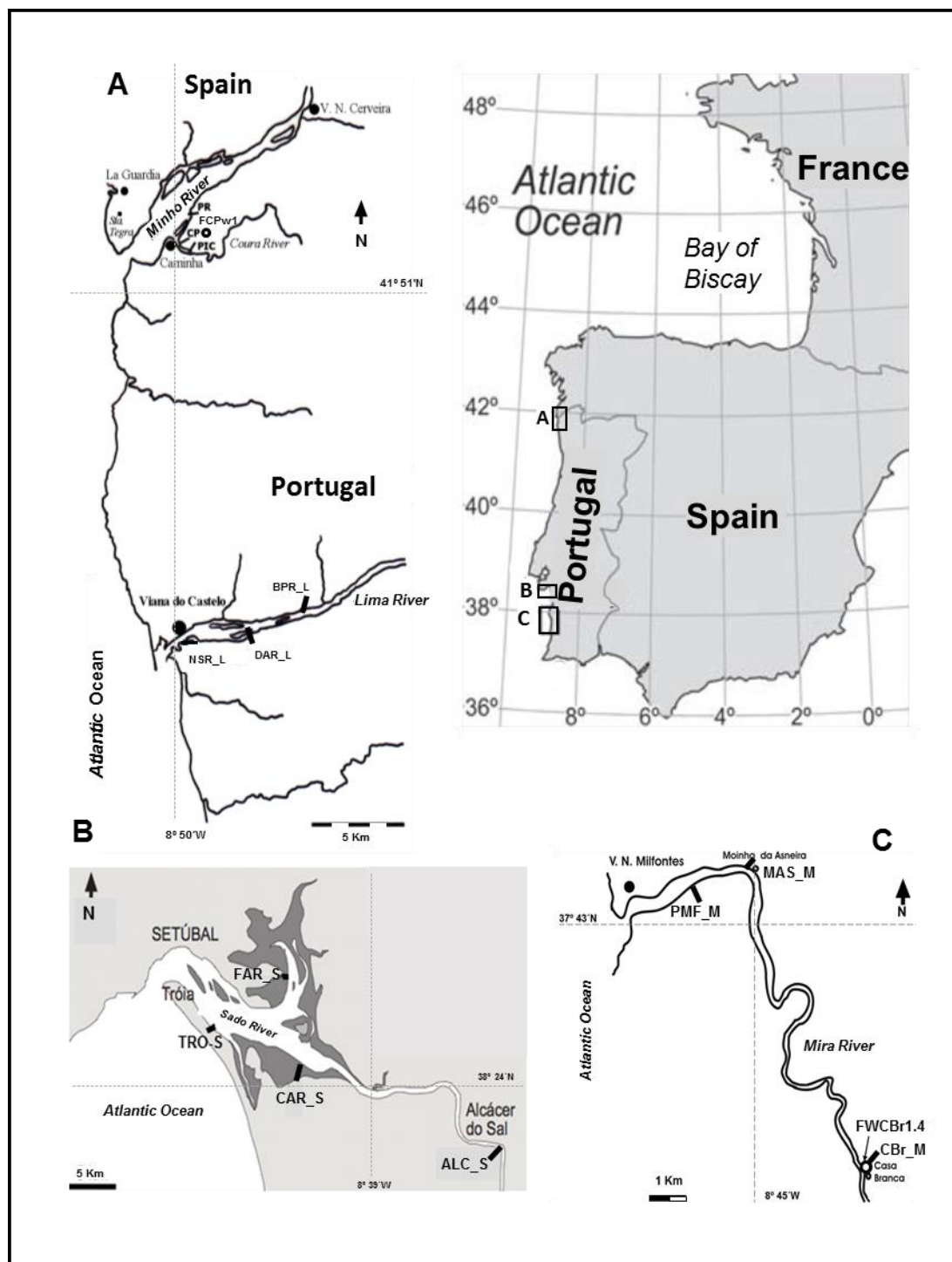
**Figure 1.** A. Study areas general location; B. Minho and Lima estuaries (NW coast); C. Sado estuary (SW coast); D. Mira estuary (SW coast). The location of the complete sampling set is also signalled. This includes thirteen surface sampling transects across the four tidal salt marshes (where both interstitial waters and sediments have been collected), and the two sediment cores obtained in the high marsh zones of the Caminha (FCPw1; Minho estuary; 1.55 m above mean sea level; 41°52′37.0″ N and 8°49′28.0″ W) and Casa Branca (FWCBr1.4; Mira estuary; 1.74 m above mean sea level; 37°40′03.7″ N and 8°43′12.7″ W) salt marshes.

55

1353
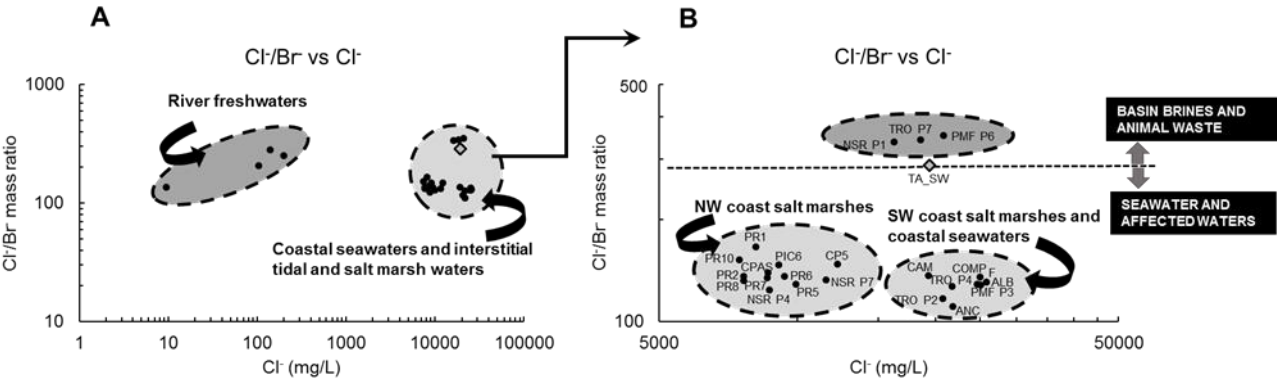


1354

Figure 2. Cl⁻/Br⁻ mass ratios vs. Cl⁻ concentrations of (surface and interstitial) water samples and potential sources (zones and theoretical limits from Panno et al., 2006). **A.** Clusters of freshwater (riverine), marine, and impacted water samples are indicated (i.e., tidal and salt marsh interstitial waters). **B.** Clusters of interstitial waters from NW and SW coastal salt marshes. Marine water samples are in the same group as the SW coast salt marshes interstitial water. A group of three anomalous samples (TRO_P7, NSR_P1 and PMF_P6) is also identified. The diamond represents a typical marine sample.
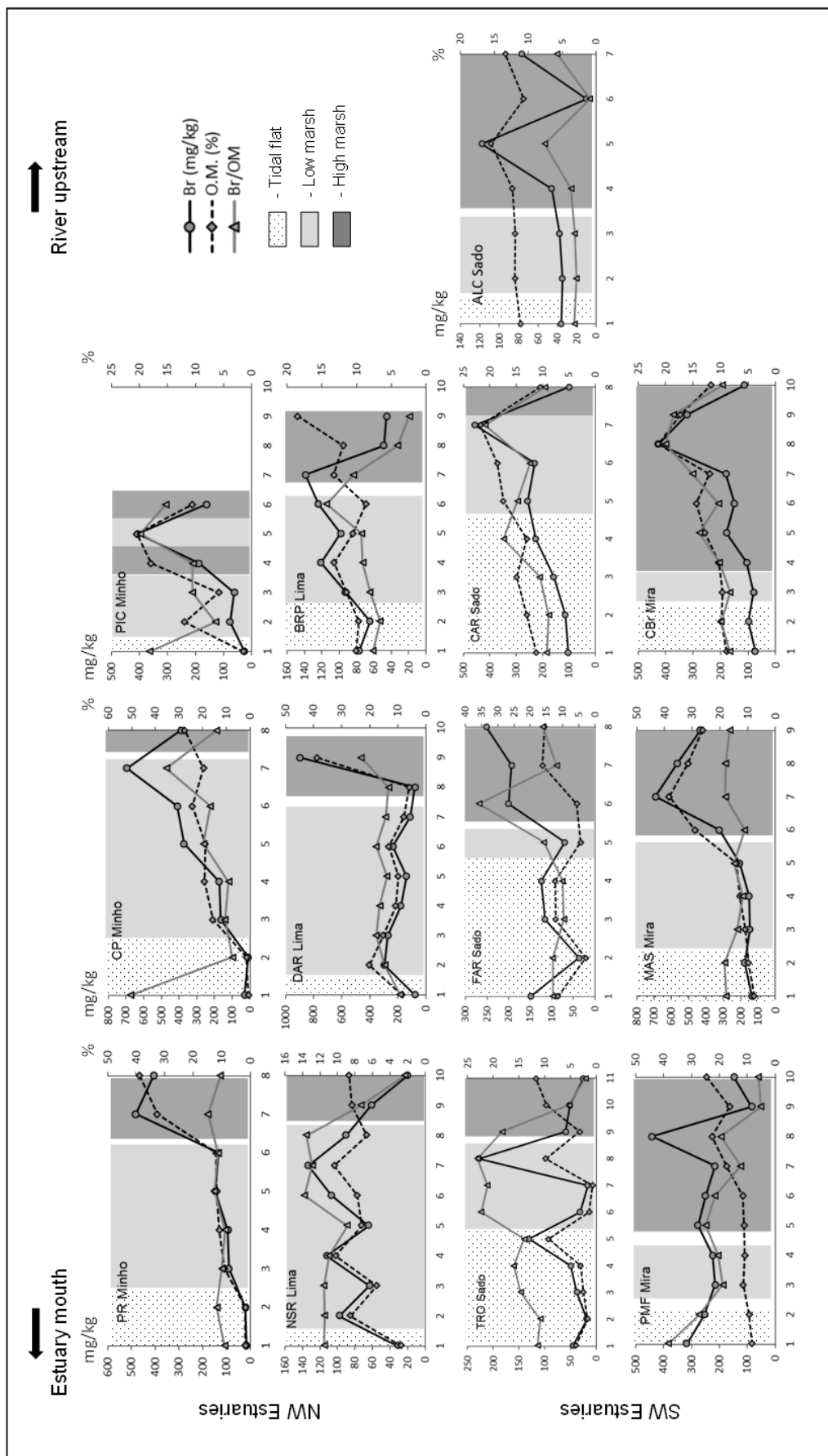
**Figure 3.** Bromine and organic matter contents (OM) of superficial tidal salt marsh sediment transects from Minho, Lima, Sado and Mira estuaries.

57
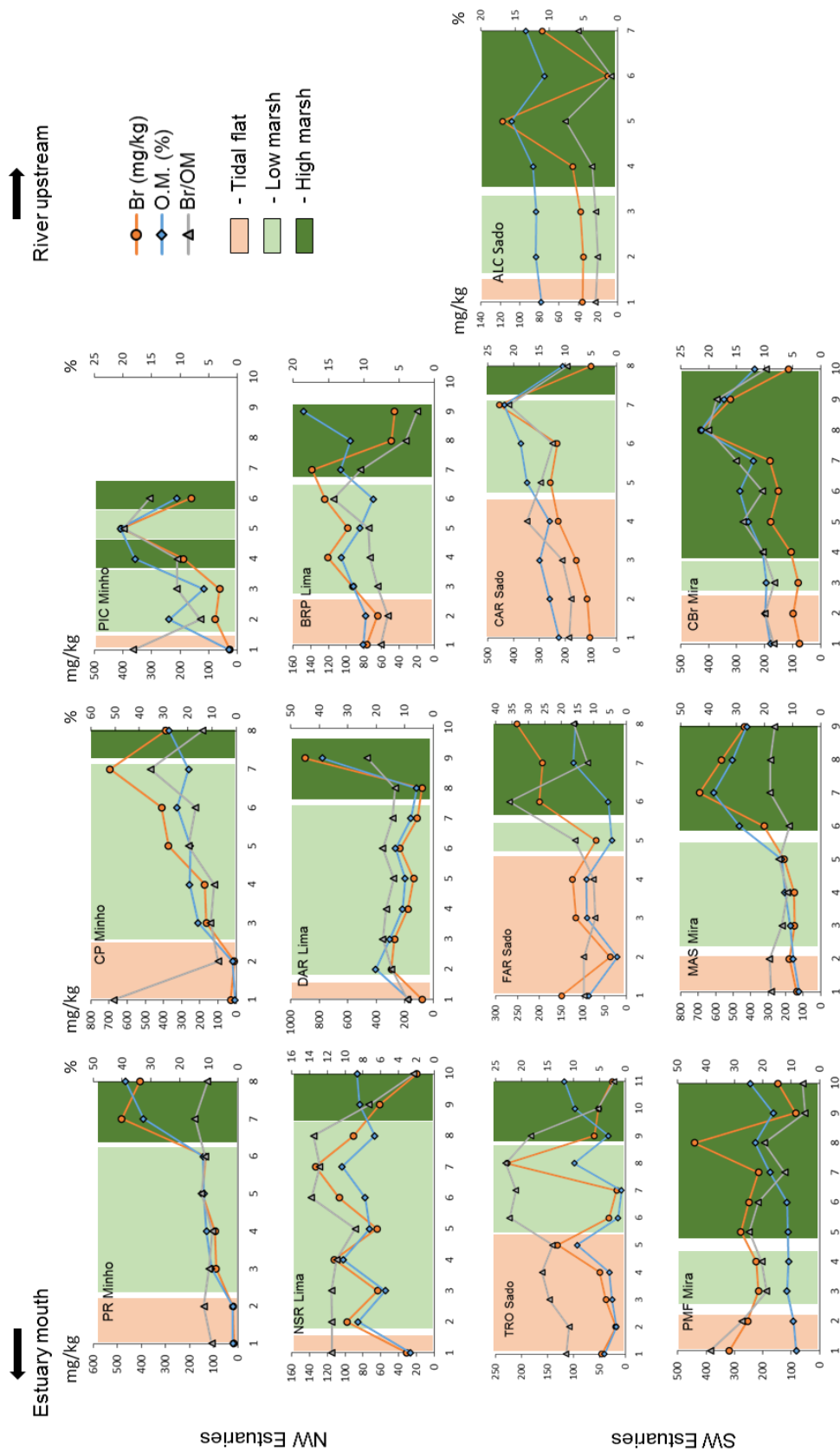
Fig 3. Bromine and organic matter (OM) contents of superficial tidal salt marsh sediment transects from Minho, Lima, Sado and Mira estuaries.
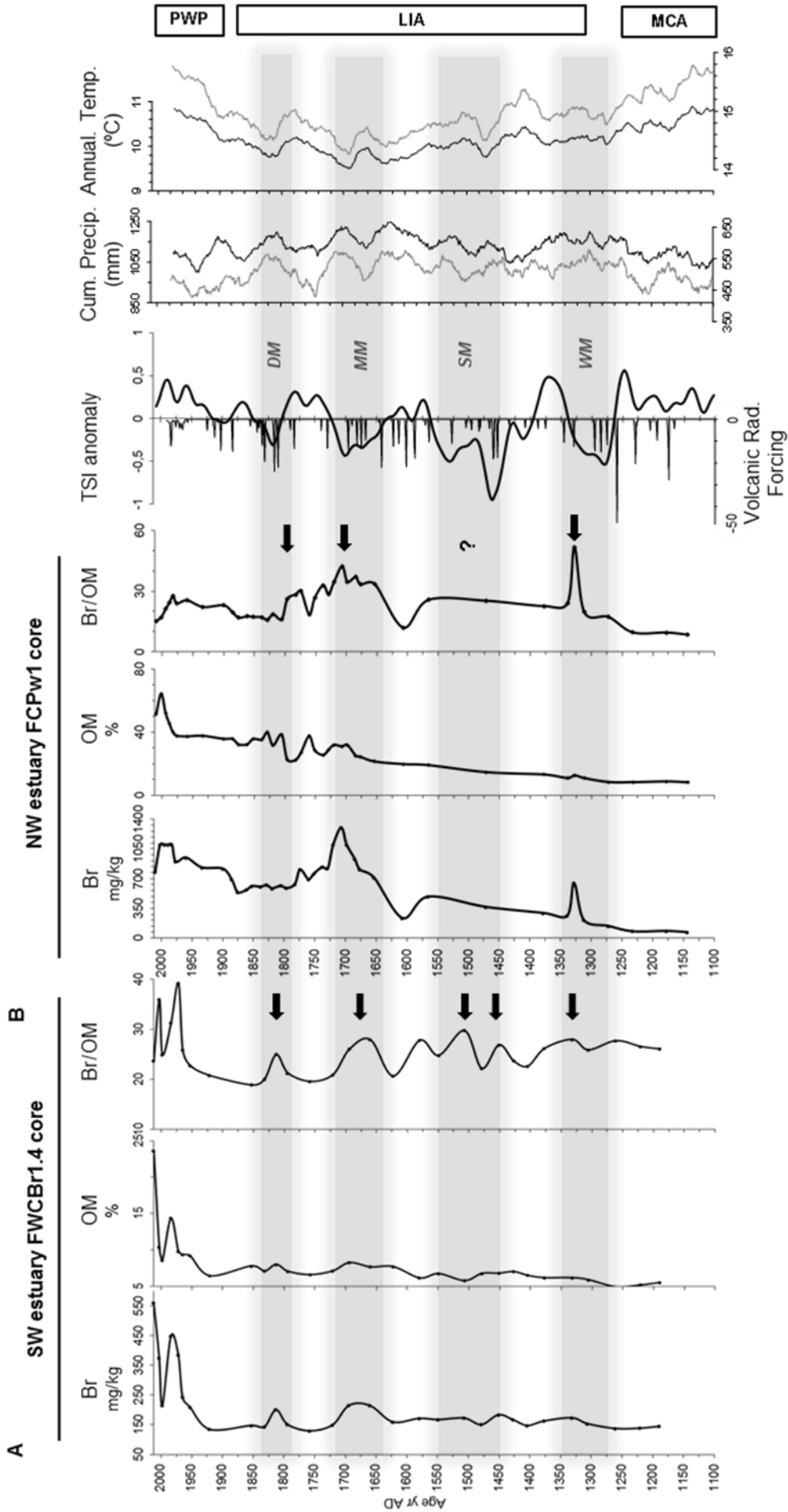
**Figure 4.** FCPw1 and FWCBr1.4 cores geochemical data: Br (mg/kg), OM (%) and Br/OM ratios. Other data represented are: TSI anomaly using a 21-year running average reconstruction (Steinhilber et al., 2012); volcanic radiative forcing (black bars) after Crowley (2000); cumulative precipitation and annual temperature (31-year running averages) for NW coast (black lines and top axis) and SW coast (grey lines and bottom axis) of Portugal (Gómez-Navarro et al., 2011). DM – Dalton Minimum; MM – Maunder Minimum; SM – Spörer Minimum; WM – Wolf Minimum.

1364

59

**Figure 5.** Conceptual model for the Br cycling in the W Portuguese coast salt marshes, including the most important elements influencing the Br pool in soils/sediments. (P– Precipitation; T– Temperature; PAR– Photosynthetically Active Radiation; ET– Evapotranspiration; S$_i$– Surface water inflow; S$_o$– Surface water outflow; G$_i$– Ground water inflow; T$_i$– Tidal water outflow; T$_o$– Tidal water outflow; [S]– Salinity; [OM]– Soil/Sediment Organic Matter content; [Br$_{org}$]– Soil/Sediment Organic Bromine content).

**Table 1.** Bromide concentrations in surface water (river freshwater, estuarine and coastal seawater) samples and in marsh interstitial water samples (Minho, Lima, Sado and Mira tidal salt marshes).

60

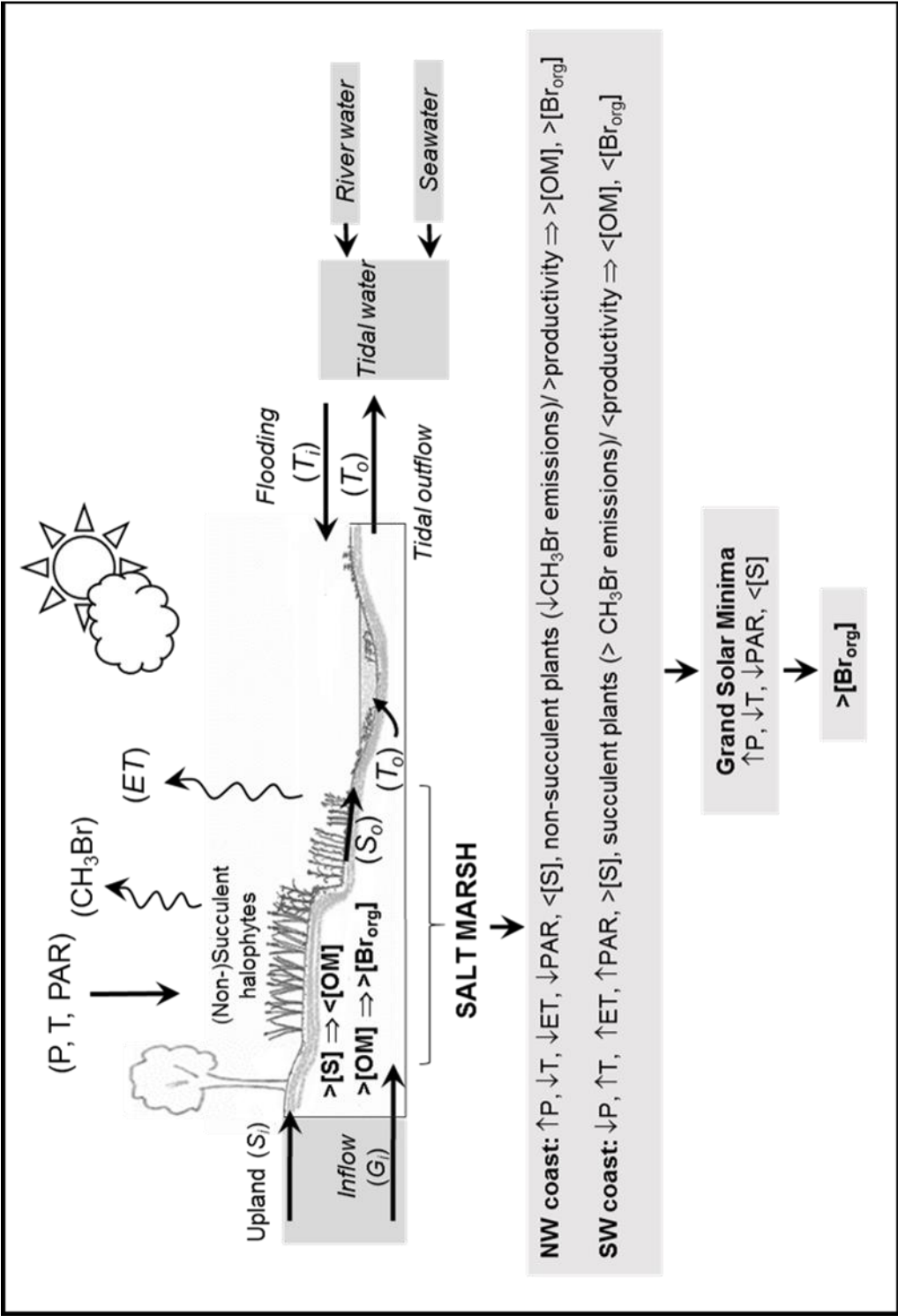| Surface and interstitial waters | NW coast | | | | SW coast | | | |
|---|---|---|---|---|---|---|---|---|
| | Minho | | Lima | | Sado | | Mira | |
| Zone | Br⁻ (mg/L) | Salinity (‰) | Br⁻ (mg/L) | Salinity (‰) | Br⁻ (mg/L) | Salinity (‰) | Br⁻ (mg/L) | Salinity (‰) |
| River | <d.l. | 0.0 | 0.07 | 0.0 | 0.8 | 0.3 | 0.5 | 0.2 |
| Estuary mouth | 141 | 32.5 | — | — | — | — | — | — |
| Coastal seawater | 197 | 35.2 | 197 | 35.2 | 185 | 35.7 | 197 | 35.4 |
| Tidal flat | 52 (48-55)* | 9.5 (2-17)* | 48 | 24.6 | 177 | 31.8 | — | — |
| Low marsh | 71 (64-83)* | 14.5 (10-18)* | 70 | 14.4 | 171 | 31.4 | 195 | 37.0 |
| High marsh | 56 (49-62)* | 12.6 (11-15)* | 87 | 13.5 | 54 | 26.6 | 59 | 30.6 |
| Marsh transect references | PR; CP; PIC | | NSR-L | | TRO-S | | PMF-M | |
| Distance to river mouth (km) | 3.8 - 4.8 | | 2.0 | | 14.0 | | 2.0 | |

*Average from three transects and range

d.l. detection limit (0.01 mg/L Br⁻)

1375

1376

1377

1378

1379 **Table 2.** Bromine content and OM contents in the surface sediment cross shore transects from the Minho,
1380 Lima, Sado and Mira intertidal domains (tidal flat, low marsh and high marsh).

1381

| Surface sediment samples / Estuaries | NW coast | | | | SW coast | | | |
|---|---|---|---|---|---|---|---|---|
| | Minho | | Lima | | Sado | | Mira | |
| Zone | Br (mg/kg) | OM (%) | Br (mg/kg) | OM (%) | Br (mg/kg) | OM (%) | Br (mg/kg) | OM (%) |
| Tidal Flat | 21 (11-30)* | 1.4 (0.6-1.7)* | 71 (31-79)* | 8.6 (2.7-10.1)* | 83 (19-226)** | 11.5 (1.7-15.0)** | 158 (75-318)* | 8.8 (7.7-9.9)* |
| Low Marsh | 133 (62-695)* | 15.0 (5.9-24.4)* | 110 (64-296)* | 11.0 (5.5-20.2)* | 53 (17-456)** | 8.2 (0.8-21.8)** | 152 (80-224)* | 11.2 (9.7-12.8)* |
| High Marsh | 389 (162-482)* | 27.7 (10.6-38.8)* | 49 (45-900)* | 13.3 (5.9-38.9)* | 81 (10-252)** | 11.7 (3.3-16.3)** | 233 (85-693)* | 16.9 (11.2-38.3)* |
| Marsh transect/cores surface references | PR; CP; PIC | | NSR_L; DAR_L; BPR_L | | TRO_S; CAR_S; FAR_S; ALC_S | | PMF_M; MAS_M; CBr_M | |
| Distance to river mouth (km) | 3.8 - 4.8 | | 2; 5; 8.5 | | 14; 19; 24; 43.5 | | 2; 3.5; 13 | |
| Correlation coeficient Br vs.OM (p < 0.001) | 0.86 (N= 21) | | 0.89 (N= 28) | | 0.67 (N= 34) | | 0.79 (N= 29) | |

*Average (median) from three transects and range
1382 **Average (median) from four transects and range

1383

| Depth (cm) | $^{137}$Cs | 2-sigma | $^{210}$Pb | 2-sigma | $^{214}$Pb | 2-sigma | $^{210}$Pb$_{excess}$ |
|---|---|---|---|---|---|---|---|
| 0.5 | 5.56 | 2.27 | 152.5 | 30.6 | 37.5 | 6.76 | 115 |
| 1.5 | 5.44 | 1.6 | 84.52 | 20.11 | 40.02 | 3.78 | 44.5 |
| 2.5 | 6.95 | 1.63 | 72.48 | 20.36 | 38.38 | 3.9 | 34.1 |
| 3.5 | 8.78 | 2.13 | 98.24 | 21.85 | 37.22 | 5.58 | 61.02 |
| 4.5 | 10.64 | 2.18 | 70.55 | 21.47 | 34.65 | 5.25 | 35.9 |
| 5.5 | 13.23 | 2.23 | 53.13 | 21.05 | 32.45 | 4.79 | 20.68 |
| 6.5 | 19.19 | 2.32 | 48.51 | 25.88 | 34.29 | 3.97 | 14.22 |
| 7.5 | 23.69 | 2.73 | 46.97 | 17.43 | 36.53 | 6.44 | 10.44 |
| 8.5 | 14.41 | 2.04 | 54.26 | 18.92 | 42.94 | 5.77 | 11.32 |
| 9.5 | 6.74 | 1.81 | 58.57 | 20.37 | 41.42 | 4.24 | 17.15 |
| 10.5 | 6.4 | 1.72 | 52.57 | 18.23 | 40.33 | 4.8 | 12.24 |
| 11.5 | 5.45 | 1.65 | 65.43 | 19.23 | 41.41 | 3.99 | 24.02 |
| 12.5 | 2.92 | | 65.13 | 22.17 | 47.18 | 4.21 | 17.95 |
| 13.5 | 2.37 | | 53.57 | 21.12 | 51.31 | 5.19 | 2.26 |
| 14.5 | 2.58 | | 56.08 | 21.57 | 52.17 | 5.83 | 3.91 |
| 15.5 | 2.5 | | 41.48 | 19.35 | 43.05 | 4.29 | -1.57 |

Pb and Cs isotopes contents (Bq kg−1)



FWCBr core age model

Appendix A. Age model for the core FWCBr and estimated 2 σ errors, based on two AMS $^{14}$C dates, performed on total organic sediment, and $^{210}$Pb and $^{137}$Cs chronology. The data interpolation was obtained with Bchron 4.1 software.

| Core/Sample | Depth (cm) | δ$^{13}$C ‰ | Conventional radiocarbon age | Δ$^{14}$C ‰ | Calibrated years AD (2 Sigma range) |
|---|---|---|---|---|---|
| FW CBr 2.0 CM 70 | 69-70 | -25.0 | 720 +/- 30 BP | -85.7±3.4 | 1260 to 1295 |
| FW CBr 2.0 CM 91 | 90-91 | -25.6 | 920 +/- 30 BP | -108.2±3.3 | 1025 to 1190 |

1384

1385 **Appendix B.** Geochemical data from the sediment core FWCBr (Casa Branca salt marsh;
1386 Mira estuary).

| Depth (cm) | Br (ppm) | OM (%) | Br/OM | Age (AD years) |
|---|---|---|---|---|
| 0-1 | 560 | 23.6 | 23.7 | 2012 |
| 1-2 | 374 | 10.4 | 36.0 | 2003 |
| 2-3 | 214 | 8.6 | 24.9 | 1998 |
| 4-5 | 448 | 14.3 | 31.2 | 1984 |
| 6-7 | 385 | 9.8 | 39.3 | 1972 |
| 8-9 | 242 | 9.4 | 25.8 | 1965 |
| 10-11 | 209 | 9.2 | 22.7 | 1953 |
| 12-13 | 134 | 6.5 | 20.7 | 1921 |
| 14-15 | 147 | 7.8 | 18.8 | 1853 |
| 16-17 | 142 | 7.1 | 20.0 | 1832 |
| 18-19 | 200 | 8.0 | 24.9 | 1813 |
| 20-21 | 150 | 7.1 | 21.2 | 1794 |
| 24-25 | 129 | 6.6 | 19.5 | 1758 |
| 28-29 | 149 | 7.1 | 20.9 | 1721 |
| 31-32 | 215 | 8.3 | 26.0 | 1694 |
| 35-36 | 214 | 7.7 | 27.9 | 1660 |
| 39-40 | 159 | 7.7 | 20.6 | 1623 |
| 43-44 | 171 | 6.2 | 27.8 | 1580 |
| 47-48 | 167 | 6.7 | 24.8 | 1549 |
| 52-53 | 172 | 5.8 | 29.7 | 1507 |
| 55-56 | 150 | 6.8 | 22.1 | 1479 |
| 58-59 | 183 | 6.8 | 26.9 | 1451 |
| 61-62 | 166 | 7.0 | 23.6 | 1427 |
| 64-65 | 147 | 6.5 | 22.6 | 1404 |
| 68-69 | 162 | 6.2 | 26.2 | 1377 |
| 72-73 | 173 | 6.2 | 28.0 | 1332 |
| 75-76 | 153 | 5.9 | 25.9 | 1306 |
| 80-81 | 137 | 4.9 | 27.7 | 1261 |
| 85-86 | 138 | 5.2 | 26.5 | 1221 |
| 89-90 | 144 | 5.5 | 26.0 | 1190 |

1387

1388

1389

1390

1391